Revised Enskog Theory (RET) and molecular dynamics simulations of the viscosities and thermal conductivity of the hard sphere fluid and crystal

Sławomir Pieprzyk* and Arkadiusz C. Brańka†
Institute of Molecular Physics, Polish Academy of Sciences,
M. Smoluchowskiego 17, 60-179 Poznań, Poland

David M. Heyes‡
Department of Physics, Royal Holloway, University of London, Egham, Surrey, TW20 0EX, United Kingdom

Marcus N. Bannerman§
School of Engineering, University of Aberdeen, AB24 3UE, United Kingdom

Hard sphere (HS) shear, longitudinal, cross and bulk viscosities and the thermal conductivity are obtained by molecular dynamics (MD) simulations, covering the entire density range from the dilute fluid to the solid crystal near close packing. The transport coefficient data for the HS crystal are largely new and display, unlike for the fluid, a surprisingly simple behavior in that they can be represented well by a simple function of the density compressibility factor.

In contrast to the other four transport coefficients (which diverge), the bulk viscosity in the solid is quite small and decreases rapidly with increasing density, tending to zero in the close packed limit. The so-called cross viscosity exhibits a different behavior to the other viscosities, in being negative over the entire solid range, and changes sign from negative to positive on increasing the density in the fluid phase.

The extent to which the viscosity tensor and thermal conductivity of the HS crystal can be represented by Revised Enskog Theory (RET) is investigated. The RET expressions are sums of an instantaneous (I), a kinetic (K) and a so-called 'α' part. The I part of the transport coefficients evaluated directly by MD are statistically indistinguishable from those of the corresponding kinetic theory (Enskog and RET) expressions. For the K part the integral over the spatial two-particle distribution function at contact was determined and the α part was estimated using the direct correlation function and density functional theory approximations.

All three parts were determined in this work which allowed the accuracy of RET for solid systems to be assessed rigorously. It is found that in the case of the thermal conductivity the predictions of RET are in excellent agreement with the MD results. Also, for the shear viscosity the agreement over the entire solid phase is quite good, but is considerably worse for the three remaining viscosities in the solid phase.

I. INTRODUCTION

When various regions of a system translate with different velocities a viscous stress arises which is proportional to the rate of change of deformation over time (strain rate). The viscosity tensor is the proportionality coefficient, which characterizes the internal friction or rate of momentum dissipation occurring in a system in response to the velocity gradients. In addition, the presence in the medium of a temperature gradient induces the transport of energy or a heat flux, which can be described by Fourier's linear relation $q_i = \lambda_{ij}\nabla_j T$, where λ_{ij} is the thermal conductivity tensor, which measures the rate of energy transfer in the medium.

The transport coefficients (TC) characterizing viscosity and thermal conductivity are the primary physical quantities of fundamental interest and practical importance in non-equilibrium studies. Kinetic theory based on the Boltzmann transport equation provides considerable insight into these TC [1]. The Boltzmann equation describes the time evolution of the single-particle velocity and position distribution function for a dilute system. The method of its solution, proposed by Chapman and Enskog, provides a basis for the computation of the viscosities, the thermal conductivities and diffusion coefficients for both simple gases and gas mixtures [1–3].

The Boltzmann equation has, however, a number of assumptions, for example, that the state of the system is described by a single-particle distribution function, and the particles move freely for most of the time and collisions between particle pairs are instantaneous. In addition it is assumed that the number of collisions which take place in small regions of space over short intervals of time can be estimated with a probabilistic assumption, the colliding particles are uncorrelated before their collision, and that no excluded volume effects are included. Consequently, Boltzmann's equation and the methods used to solve it are basically only applicable for dilute systems.

For particle systems at higher densities additional fea-

———

* slawomir.pieprzyk@ifmpan.poznan.pl
† branka@ifmpan.poznan.pl
‡ david.heyes@rhul.ac.uk
§ m.campbellbannerman@abdn.ac.uk

tures such as finite particle-size effects become relevant and should be taken into account in any realistic description. Such a generalization of Boltzmann's approach has been made for hard sphere (HS) systems and this extension is known as Enskog theory [1, 2]. The HS system aspect of this generalization means that all collisions between particles are instantaneous and binary, and the difference in location of the centers of the two colliding particles is well defined. The fact that this analytic development can be made successfully is noteworthy. The essence of Enskog's theory is to assume that there is a velocity-independent spatial correlation between particles which is specified by the spatial pair correlation function for an equilibrium system with a uniform density. The Enskog method was used to derive formulas for the density dependence of the shear and bulk viscosities, thermal conductivity and self-diffusion coefficient [1, 2, 4]. A comparison with 'exact' molecular dynamics simulation results has demonstrated that Enskog's formulas describe the transport properties of the HS fluid very well and the observed differences at higher fluid densities can be ascribed mainly to the fact that Enskog theory, like the Boltzmann approach, ignores velocity correlations between the colliding particles.

A more general approach known as 'Revised Enskog Theory' (RET) was proposed by van Beijeren and Ernst [5] in which the original Enskog equation was replaced by one in which a spatially dependent pair distribution function for the particles was used. With RET a more accurate description of the transport coefficients of gas mixtures was obtained [5–7].

In 1990 Kirkpatrick *et al.* [8] used the RET approach to derive the dissipative linear equations of elasticity and obtained expressions for the corresponding transport coefficients. It is expected that these expressions may be exploited to describe a hard sphere crystal. These formulas are however, given in terms of integrals involving a multidimensional, anisotropic pair correlation function and thus are somewhat formal and the practicalities of evaluating them were not considered.

This possible extension of kinetic theory to a crystal has yet to be tested, as far as we are aware, mainly due to the lack of a molecular dynamics (MD) simulation data for the HS crystal TC and problems with obtaining reliable results for the solid pair correlation function and the components of the elastic moduli tensor required in the theory.

This work addresses these issues by achieving two main goals. First, 'exact' simulation data for the viscosity tensor and thermal conductivity over the entire density range of the HS system (with a focus on the crystal) is determined by MD here. Secondly, the corresponding RET expressions for the transport coefficients and their various parts are calculated. It is by accomplishing these two steps that the extent to which transport in the HS solid can be described by RET can be assessed.

This study is organized as follows. In Section II the MD calculation details of the TC of the hard sphere system are described. The revised Enskog theory is discussed in Section III. In Section IV the main results for the hard sphere fluid and solid are presented, also in this section the revised Enskog theory is checked for accuracy for the various elements of the viscosity tensor. The main conclusions of the analysis are summarized in Section V.

II. MD CALCULATIONS OF THE TC

The solid HS structure is the fcc crystal for which the viscosity tensor can be written as the general formula [8, 9]

$$\eta_{ijkl} = \eta_1(\delta_{ik}\delta_{jl} + \delta_{il}\delta_{jk} - \delta_{ij}\delta_{kl}) + \eta_2\delta_{ij}\delta_{kl} + \eta_3\delta_{ijkl}^{(4)}, \quad (1)$$

where η_p, $(p = 1, 2, 3)$ are scalars which we will be referred to as the p-viscosities or just 'viscosities', δ_{ij} is the Kronecker symbol, $\delta_{ijkl}^{(4)}$ is a cubic invariant tensor which is equal to unity if all indices are the same and otherwise is zero. Each index represents here a Cartesian component e.g., $i = x$, or y, or z. There are therefore for cubic symmetry three nonzero independent components: (a) $\eta_{xxxx} = \eta_{yyyy} = \eta_{zzzz}$, (b) $\eta_{xxyy} = \eta_{xxzz} = ... = \eta_{yyzz}$ and (c) $\eta_{xyxy} = ...$ which in the Voigt notation [10] are,

$$\eta_{11} = \eta_{xxxx} = \eta_1 + \eta_2 + \eta_3, \quad (2a)$$
$$\eta_{12} = \eta_{xxyy} = \eta_2 - \eta_1, \quad (2b)$$
$$\eta_{44} = \eta_{xyxy} = \eta_1. \quad (2c)$$

The viscosity, η_{12}, does not appear to have a name in the literature, and we refer to it here as the 'cross' viscosity.

The definitions of the p-viscosities in terms of the quantities in Eq. (2) are,

$$\eta_1 = \eta_{44}, \quad (3a)$$
$$\eta_2 = \eta_{12} + \eta_{44}, \quad (3b)$$
$$\eta_3 = \eta_{11} - \eta_{12} - 2\eta_{44}. \quad (3c)$$

For a fluid, the customary notation $\eta_S = \eta_{44}$ for the shear viscosity and $\eta_L = \eta_{11}$ for the longitudinal viscosity will also be used.

In isotropic liquid systems only two components are independent and these are sufficient to characterize the viscosity tensor [9, 11]. These can be any pair of the η_{ij} viscosities (where the index ij denotes the case of 11, 12 or 44 viscosity) but the most frequently employed are those used with the Navier-Stokes equations i.e., the shear viscosity η_S, and the bulk viscosity η_B which can be expressed in terms of the other viscosity tensor components. It is noteworthy that in a fluid because of the isotropic condition, $\eta_{11} - \eta_{12} - 2\eta_{44} = 0$ (which follows directly from Eq. (3c) for $\eta_3 = 0$ in fluid) and consequently the bulk viscosity can be defined in three ways: $\eta_B = \eta_{11} - 4\eta_{44}/3 = \eta_{12} + 2\eta_{44}/3 = (\eta_{11} + 2\eta_{12})/3$. The first equality is often used, probably because the cross-viscosity is more difficult to determine by experiment,

and it has to be obtained indirectly from the other measurable viscosities (i.e., the shear and bulk) anyway. For the crystal where the isotropic condition does not arise, the expression for the bulk viscosity [9] is,

$$\eta_B = \frac{1}{3}\left(\eta_{11} + 2\eta_{12}\right) = \frac{1}{3}\left(-\eta_1 + 3\eta_2 + \eta_3\right). \quad (4)$$

Also due to the cubic symmetry, the thermal conductivity $\lambda_{ij} = \lambda\delta_{ij}$ i.e., is described by a scalar.

Both the viscosities and thermal conductivity can be evaluated with the molecular dynamics simulation methods [12, 13]. Because of the non-analytic nature of the HS interaction, the transport coefficients of the HS system are determined through the Einstein-Kubo-Helfand (EKH) approach [9, 14, 15], instead of the conventional Green-Kubo method [12]. The EKH expressions are formulated in terms of averages of the Helfand moments,

$$L_{\alpha,\beta}(\Delta t) = \mathcal{A}\left\langle G_\alpha(t_0 + \Delta t)G_\beta(t_0 + \Delta t)\right\rangle_{t_0}, \quad (5)$$

where Δt is the correlation time, $\mathcal{A} = 1/2Vk_BT^2\Delta t$ for the thermal conductivity and $\mathcal{A} = 1/2Vk_BT\Delta t$ for the viscosities. The volume of the system is V, k_B is the Boltzmann constant, and $T = 1$ is the temperature. The angular brackets $\langle\ldots\rangle_{t_0}$ denote an average over time origin, t_0. The Helfand moment is defined as the integral of the microscopic flux over a number of collisions, and is composed of kinetic and potential terms $G_\alpha(t_0 + \Delta t) = G_\alpha^{(k)}(t_0 + \Delta t) + G_\alpha^{(c)}(t_0 + \Delta t)$ collected in Table I for the considered transport coefficients, from which the kinetic kk, interaction cc, and cross kc parts of the transport coefficients can be obtained: η_{ij}^{kk}, η_{ij}^{cc}, η_{ij}^{kc} and λ^{kk}, λ^{cc}, λ^{kc}. The index, α, β, refer to the calculated quantity (first column in Table I). For example shear viscosity can be calculated as follows $\eta_{44} = \eta_{xyxy} = L_{\eta_{xy},\eta_{xy}}$, where $L_{\eta_{xy},\eta_{xy}} = 1/2Vk_BT\Delta t\left\langle G_{\eta_{xy}}(t_0 + \Delta t)G_{\eta_{xy}}(t_0 + \Delta t)\right\rangle_{t_0}$ and $G_{\eta_{xy}}(t_0 + \Delta t) = G_{\eta_{xy}}^{(k)}(t_0 + \Delta t) + G_{\eta_{xy}}^{(c)}(t_0 + \Delta t)$. The thermal conductivity can be defined in the same way.

The transport coefficients of the HS system can also be decomposed into the sum of a singular and non-singular part, which is a unique feature of hard sphere and other discontinuous hard core potential systems [16–19]. The singular or 'instantaneous' part of the transport coefficient represents contributions to G at the time $(t \to 0)$ when the first collision takes place and in this work the latter name will be used because it more clearly indicates the physical origin of the term. Exact formulas for the instantaneous part of the viscosities which can be computed directly in the simulations, have been derived recently [16, 20],

$$\eta_S^{(I)} = \frac{m^2}{2Vk_BT\Delta t}\left\langle b_0^2 \frac{r_{ij,x}r_{ij,y}}{r_{ij}}\frac{r_{ij,x}r_{ij,y}}{r_{ij}}\right\rangle, \quad (6a)$$

$$\eta_{12}^{(I)} = \frac{m^2}{2Vk_BT\Delta t}\left\langle b_0^2 \frac{r_{ij,x}r_{ij,x}}{r_{ij}}\frac{r_{ij,y}r_{ij,y}}{r_{ij}}\right\rangle, \quad (6b)$$

TABLE I. The terms in the EKH formulas in Eq. (5) for the viscous stress and heat flux terms. The sum $\sum_{i,j}^{coll}$ is over all interacting ij pairs of particles in the time interval $[t_0, t_0 + \Delta t]$, *coll* is the number of collisions, e_i is the internal energy of i-th particle, $\Delta v_{i,x}$ is the x Cartesian component of the velocity change of i-th particle, and Δe_i is the internal energy change after and before a collision of i-th particle. The α in the column headings represents in a generic way the component of the thermal conductivity or viscosities for different combinations of the Cartesian components.

α	$G_\alpha^{(k)}(t_0 + \Delta t)$	$G_\alpha^{(c)}(t_0 + \Delta t)$
λ_{xx}	$\int_{t_0}^{t_0+\Delta t}\sum_i^N v_{i,x}e_i dt$	$\sum_{i,j}^{coll} r_{ij,x}\Delta e_i$
η_{xx}	$\int_{t_0}^{t_0+\Delta t}\sum_i^N m_i v_{i,x}v_{i,x} dt$	$\sum_{i,j}^{coll} r_{ij,x}m_i\Delta v_{i,x}$
η_{xy}	$\int_{t_0}^{t_0+\Delta t}\sum_i^N m_i v_{i,x}v_{i,y} dt$	$\sum_{i,j}^{coll} r_{ij,x}m_i\Delta v_{i,y}$

$$\eta_L^{(I)} = \frac{m^2}{2Vk_BT\Delta t}\left\langle b_0^2 \frac{r_{ij,x}r_{ij,x}}{r_{ij}}\frac{r_{ij,x}r_{ij,x}}{r_{ij}}\right\rangle, \quad (6c)$$

$$\eta_B^{(I)} = \frac{m^2}{18Vk_BT\Delta t}\left\langle b_0^2\sigma^2\right\rangle, \quad (6d)$$

where m is the mass of the particle, and $b_0 = \mathbf{v}_{ij}\cdot\hat{\mathbf{r}}_{ij}$.

For thermal conductivity the instantaneous part is

$$\lambda^{(I)} = \frac{1}{6Vk_BT^2\Delta t}\left\langle\sum_{a=1}^{3}[r_{ij,a}\Delta e_i]^2\right\rangle, \quad (6e)$$

where the internal energy of i-th particle is $e_i = \sum_{a=1}^{3} p_{i,a}^2/2m$, and $\Delta e_i = e_i^+ - e_i^-$ where $+$ and $-$ indicate after and before the collision, respectively. In the calculations, $\hat{\mathbf{r}}_{ij} = \mathbf{r}_{ij}/r_{ij}$ is the unit vector, where $\mathbf{r}_{ij} = \mathbf{r}_i - \mathbf{r}_j$ is the vector between the HS i and j particle positions, and $r_{ij,x}$, $r_{ij,y}$, $r_{ij,z}$ are the distances between ij particles in cartesian coordinates on collision. $\mathbf{v}_{ij} = \mathbf{v}_i - \mathbf{v}_j$ is the velocity difference between HS particles.

As will be shown below the ability now to evaluate these instantaneous viscous quantities is crucial to describe fully transport properties in the HS crystal.

The transport coefficient calculations were performed mainly using the DynamO program [21] employing different system sizes, $N = 2048, 4000, 8788, 16384, 37044$ and 131072 particles in a cubic simulation box, under periodic boundary conditions [12]. In these simulations the system was equilibrated for 10^5 collisions per particle, and then production data were collected over the following 1.5×10^6 collisions per particle (which means 1.64×10^9 equilibrated collisions, and 2.46×10^{10} collisions in total in the case of N=16384). The chosen equilibration time

is sufficient to ensure that the considered transport quantities are free from the influence of the initial parameters. Each simulation was conducted at least $10 - 20$ times to improve the statistics, and each density was started with a different set of initial random velocities. Statistical errors in all simulation property averages were estimated by the block average method [12]. Some calculations were performed also with a home-made code, e.g., to compute the instantaneous parts of viscosities and thermal conductivity.

In the case of the transport coefficients the N-dependence may be quite significant even for quite large systems e.g., in the case of the self-diffusion coefficient (D) the dependence is $\sim N^{-1/3}$ [22–25]. Thus, a careful check of the system size dependence of viscosities is needed to determine the thermodynamic limit values, especially as an oscillatory behavior at smaller N in the value of the shear viscosity has been observed [26]. The present MD calculations indicate that the HS viscosities, η_{ij}, approach the thermodynamic limit as $\sim N^{-1}$. In the case of thermal conductivity, this dependence is $\sim N^{-2/3}$, as was shown previously [27]. The present calculations show that this slower convergence comes from the non-singular part of thermal conductivity as the instantaneous part has an $N-$dependence of the type $\sim N^{-1}$, typical of thermodynamic and mechanical properties [13]. Details of the system size dependence of the studied quantities are given in the Appendix A. All of the MD HS transport coefficients for the fluid and solid presented in this work are the values obtained by extrapolating to the thermodynamic limit.

III. RET DESCRIPTION OF THE TRANSPORT PROPERTIES OF A HARD SPHERE CRYSTAL

The revised Enskog equation is an extension of the Enskog kinetic equation by considering the special correlation between particles through the position dependent two-particle distribution function [5]. It is expected that with this approach a nonuniform system may be approximately described. Kirkpatrick *et al.* [8] derived from the linearized revised Enskog kinetic equations, the dissipative linearized equations of elasticity for the displacement and temperature fields. With these equations a number of expressions for the TC of the ideal (fcc) hard sphere crystal were derived in terms of the (solid state) equilibrium two-particle distribution function at contact, which are presented below.

In the case of the thermal conductivity, the derived expression is shown to consist of two parts: the instantaneous ('I') contribution,

$$\lambda^{(I)} = \lambda_{00} b_2 \frac{32}{25\pi} \rho \mathcal{Z}, \qquad (7)$$

where

$$\lambda_{00} = \frac{75 k_B}{64 \sigma^2} \left(\frac{k_B T}{m\pi} \right)^{1/2}, \qquad (8)$$

$b_2 = 2\pi\sigma^3/3$ is the second virial coefficient of the hard sphere system, $\rho = N/V$ is the number density, and σ is the sphere diameter; and the kinetic ('K') contribution,

$$\begin{aligned}
\lambda^{(K)} = \lambda_0 b_2 \rho \mathcal{Z} & \left[\frac{1}{\mathcal{Z}^2} + \frac{6}{5\mathcal{Z}} + \frac{9}{25} \right. \\
& - \left(\frac{1}{3\mathcal{Z}^2} + \frac{2}{5\mathcal{Z}} + \frac{3}{25} \right) X + \left(\frac{8}{15\mathcal{Z}} + \frac{32}{75} \right) X^2 \right] \\
& \times \left(1 - \frac{X}{3} - \frac{2X^2}{3} \right)^{-1},
\end{aligned} \qquad (9)$$

where $\lambda_0 = 1.02522\lambda_{00}$, and 1.02522 is the Sonine polynomial correction factor [2, 28]. The 'normalized' function $X = F'/\mathcal{Z}$ is used in the above equation. Note we use $\mathcal{Z}$ (i.e., the nonideal gas part of the equation of state compressibility factor of the HS crystal) for the symbol F_1 in Ref. 8.

The F' function has the following definition [8],

$$F' = \frac{\sigma^3}{4\rho V} \int d\mathbf{r}_1 d\hat{\sigma} (5\hat{\sigma}_x^4 - 1) \varrho(\mathbf{r}_1) \varrho(\mathbf{r}_1 - \sigma\hat{\sigma}) G_2(\mathbf{r}_1, \mathbf{r}_1 - \sigma\hat{\sigma}), \qquad (10)$$

where $\varrho(\mathbf{r}_1)$ is the one-particle density distribution function and $\varrho(\mathbf{r}_1)\varrho(\mathbf{r}_1 - \sigma\hat{\sigma})G_2(\mathbf{r}_1, \mathbf{r}_1 - \sigma\hat{\sigma})$ is related to the equilibrium spatial two-particle distribution function at contact. For the isotropic liquid, $F' = 0$ ($X = 0$), and the sum of the above expressions in Eqs. (7) - (9) reduces to the Enskog formula given in Eq. (25e) below. Thus, F' can be considered to be a measure of the structural and indirectly the dynamical anisotropy in the HS crystal.

It is worth recalling [1] that RET theory, like the kinetic theory of gases, ignores the effects of correlated motion e.g., it assumes no velocity correlation between particles before the collision takes place (the recollision is absent). Consequently, the true or exact expression for λ is

$$\lambda = \lambda^{RET} + \lambda^{(Q)} = \lambda^{(I)} + \lambda^{(K)} + \lambda^{(Q)}, \qquad (11)$$

where the residual part, denoted by a 'Q' superscript, $\lambda^{(Q)}$, represents all contributions not included in the RET expression (such as contributions which comes from any effects due to velocity correlations between particles that exist before their collision, recollisions or cyclic collisions and many-particle collisions [1]). When the ratio, $\lambda/\lambda^{RET} \approx 1$ the contribution of $\lambda^{(Q)}$ is either small or the various effects mutually cancel out, in which case the revised kinetic theory description is then adequate. This is the situation observed for the HS fluid where the representation of λ by λ^E (in Eq. (25e)) is within 5 % even in the dense fluid region [27, 29]. In the case of the HS solid the contribution of $\lambda^{(Q)}$ is unknown and will be considered in Section IV.

An assessment of this residual part will enable conclusions to be made about the performance of the RET in the case of the thermal conductivity of the HS crystal. Also, note that the key to achieving such an assessment is the determination of F' defined in Eq. (10).

In the case of the viscosity tensor,

$$\eta_p = \eta_p^{RET} + \eta_p^{(Q)}, \qquad (12)$$

where $p = 1, 2, 3$ and each RET p-viscosity component is a sum of three parts [8],

$$\eta_p^{RET} = \eta_p^{(I)} + \eta_p^{(K)} + \eta_p^{(\alpha)}. \qquad (13)$$

The instantaneous part of the viscosities is,

$$\begin{aligned}
\eta_1^{(I)} &= \eta_{00} b_2 \frac{48}{25\pi} \rho(\mathcal{Z} - F') \\
&= \eta_{00} b_2 \frac{48}{25\pi} \rho \mathcal{Z}(1 - X),
\end{aligned} \qquad (14a)$$

$$\eta_2^{(I)} = 2\eta_1^{(I)}, \qquad (14b)$$

$$\eta_3^{(I)} = \eta_{00} b_2 \frac{96}{10\pi} \rho F' = \eta_{00} b_2 \frac{96}{10\pi} \rho \mathcal{Z} X, \qquad (14c)$$

where

$$\eta_{00} = \frac{5}{16\sigma^2} \left(\frac{mk_B T}{\pi} \right)^{1/2}. \qquad (15)$$

The kinetic part is

$$\begin{aligned}
\eta_1^{(K)} &= \eta_0 b_2 \rho \frac{1 + \frac{4}{5}(\mathcal{Z} - F') + \frac{4}{25}(\mathcal{Z} - F')^2}{Z + \frac{2}{3}F'} \\
&= \eta_0 b_2 \rho \mathcal{Z} \frac{\frac{1}{\mathcal{Z}^2} + \frac{4}{5\mathcal{Z}}(1 - X) + \frac{4}{25}(1 - X)^2}{1 + \frac{2}{3}X}
\end{aligned} \qquad (16a)$$

$$\eta_2^{(K)} = \frac{\eta_1^{(K)} - \eta_3^{(K)}}{3}, \qquad (16b)$$

$$\begin{aligned}
\eta_3^{(K)} &= 2\eta_0 b_2 \rho \frac{\left(1 + \frac{2}{5}\mathcal{Z} + \frac{3}{5}F'\right)^2}{\mathcal{Z} - F'} - 2\eta_1^{(K)} \\
&= 2\eta_0 b_2 \rho \mathcal{Z} \frac{\left(\frac{1}{\mathcal{Z}} + \frac{2}{5} + \frac{3}{5}X\right)^2}{1 - X} - 2\eta_1^{(K)},
\end{aligned} \qquad (16c)$$

where $\eta_0 = 1.016\eta_{00}$.

Note, that just as for the thermal conductivity case the instantaneous and kinetic parts of viscosities are functions of $\mathcal{Z}$ and F' (or X) only. The third part, $\eta_p^{(\alpha)}$ in Eq. (13) is the most complex contribution to determine. It occurs only in the solid state (in the isotropic fluid $\eta_p^{(\alpha)} = 0$) where density fluctuations on a molecular scale become a relevant macroscopic variable. The expressions derived in Ref. 8 for this part can be written in the following compact form,

$$\eta_1^{(\alpha)} = \rho \mathcal{Z} \mathcal{E}_1 \mathcal{F}_1, \qquad (17a)$$

$$\eta_2^{(\alpha)} = \eta_1^{(\alpha)} + \rho \mathcal{Z} \mathcal{E}_2 \mathcal{F}_2 - \rho \mathcal{Z} \mathcal{E}_3 \mathcal{F}_3, \qquad (17b)$$

$$\eta_3^{(\alpha)} = -2\eta_1^{(\alpha)} + 3\rho \mathcal{Z} \mathcal{E}_3 \mathcal{F}_3, \qquad (17c)$$

where the $\mathcal{E}_p$ represent the elastic terms and $\mathcal{F}_p$ are mainly from the dissipative part calculations. Note that $\eta_p^{(\alpha)}$, just as for the instantaneous and kinetic parts are proportional to the factor $\rho \mathcal{Z}$. The pure elastic terms $\mathcal{E}_1 = C_{44}^{u\alpha}/C_{44}^{\alpha\alpha}$, $\mathcal{E}_2 = (C_{11}^{u\alpha} + 2C_{12}^{u\alpha})/(C_{11}^{\alpha\alpha} + 2C_{12}^{\alpha\alpha})$ and $\mathcal{E}_3 = (C_{11}^{u\alpha} - C_{12}^{u\alpha})/(C_{11}^{\alpha\alpha} - C_{12}^{\alpha\alpha})$, are the combinations of the density functional theory (DFT) components of the elastic moduli tensor. The elastic terms can be expressed in terms of the equilibrium solid state two-particle direct correlation function (DCF) (see Appendix B in Ref. 8) or by the approximate DFT expressions [30]. The first approach is largely formal as for the crystal the two-particle DCF is a structural quantity which is very difficult to obtain in practice and only recently, in Ref. 31 has the possibility of determining it been attempted. Some discussion on estimating the elastic terms from the DCF approach in the dense crystal limit is given in Appendix D. The second approach based on the DFT approximation is more feasible but less accurate, and limited to a specific density range which is discussed in Appendix C.

The $\mathcal{F}_p$ functions in Eqs. (17) are,

$$\begin{aligned}
\mathcal{F}_1 = \eta_{00} \frac{16}{5} W \Bigg[&\frac{1}{5}\left(1 - \bar{X}\right) \\
&- \frac{\pi}{16}\left(\frac{1}{\mathcal{Z}} + \frac{2}{5}(1 - X)\right)\frac{\frac{3}{2} + \bar{X}}{\frac{3}{2} + X} \Bigg],
\end{aligned} \qquad (18a)$$

$$\mathcal{F}_2 = \eta_{00} \frac{16}{15} W, \qquad (18b)$$

$$\begin{aligned}
\mathcal{F}_3 = \eta_{00} \frac{16}{15} W \Bigg[&\left(\frac{2}{5} + \frac{3}{5}\bar{X}\right) \\
&- \frac{\pi}{8}\frac{1 - \bar{X}}{1 - X}\left(\frac{1}{\mathcal{Z}} + \frac{2}{5} + \frac{3}{5}X\right) \Bigg],
\end{aligned} \qquad (18c)$$

where, as above, $X = F'/\mathcal{Z}$ and $\bar{X} = \bar{F}'/\bar{\mathcal{Z}}$, and $W = \bar{\mathcal{Z}}/\mathcal{Z}$ are defined in terms of the $\bar{\mathcal{Z}}$, and $\bar{F}'$.

The function $\bar{\mathcal{Z}}$ is defined in Eq. (4.21a) in Ref. 8 and is,

$$\begin{aligned}
\bar{\mathcal{Z}} = \frac{a^2 \sigma^2}{6\rho V} \int d\mathbf{r}_1 d\hat{\sigma}[\hat{\sigma} \cdot \nabla_1 \varrho(\mathbf{r}_1)] \\
\times \varrho(\mathbf{r}_1 - \sigma\hat{\sigma})G_2(\mathbf{r}_1, \mathbf{r}_1 - \sigma\hat{\sigma}).
\end{aligned} \qquad (19)$$

Taking into account the fact that $\varrho(\mathbf{r})$ is represented well by the N Gaussian distributions $\pi^{-3/2}\alpha^{-3/2}a^{-3}\exp(-(\mathbf{R} - \mathbf{r})^2/a^2\alpha)$ where α describes here the (dimensionless) width of the local density distribution and $a = (4/\rho)^{1/3}$ is the real-space lattice-constant, the above quantity in Eq. (19) is,

$$\begin{aligned}
\bar{\mathcal{Z}} = -\frac{\sigma^2}{3\alpha} \int d\mathbf{r}_1 d\hat{\sigma}[\mathbf{r}_1 \cdot \hat{\sigma}] \\
\times \varrho(\mathbf{r}_1)\varrho(\mathbf{r}_1 - \sigma\hat{\sigma})G_2(\mathbf{r}_1, \mathbf{r}_1 - \sigma\hat{\sigma}).
\end{aligned} \qquad (20)$$

In the same way, Eq. (4.21b) in Ref. 8 for $\bar{F}'$ can be expressed as,

$$\bar{F}' = -\frac{\sigma^2}{2\alpha} \int d\mathbf{r}_1 d\hat{\sigma} [\mathbf{r}_1 \cdot \hat{\sigma}](5\hat{\sigma}_x^4 - 1)$$
$$\times \varrho(\mathbf{r}_1)\varrho(\mathbf{r}_1 - \sigma\hat{\sigma})G_2(\mathbf{r}_1, \mathbf{r}_1 - \sigma\hat{\sigma}). \quad (21)$$

Therefore, the evaluation of the $\mathcal{F}_p$ terms requires calculations of the quantities, F', $\bar{\mathcal{Z}}$, $\bar{F}'$, and this issue is considered in Section IV C.

The expressions in Eqs. (14) (16) and (17) are summarized below in the Voigt notation. For the instantaneous parts of the viscosities these are,

$$\eta_{44}^{(I)} = \eta_{00}b_2\rho\mathcal{Z}\frac{48}{25\pi}(1-X), \quad (22a)$$

$$\eta_{12}^{(I)} = \eta_{44}^{(I)}, \quad (22b)$$

$$\eta_{11}^{(I)} = 3\eta_{44}^{(I)} + \eta_{00}b_2\rho\mathcal{Z}\frac{96}{10\pi}X, \quad (22c)$$

$$\eta_{B}^{(I)} = \frac{5}{3}\eta_{44}^{(I)} + \eta_{00}b_2\rho\mathcal{Z}\frac{96}{30\pi}X, \quad (22d)$$

for the kinetic parts

$$\frac{\eta_{44}^{(K)}}{\rho\mathcal{Z}} = \eta_0 b_2 \frac{\frac{1}{\mathcal{Z}^2} + \frac{4}{5\mathcal{Z}}(1-X) + \frac{4}{25}(1-X)^2}{1 + \frac{2}{3}X}, (23a)$$

$$\frac{\eta_{12}^{(K)}}{\rho\mathcal{Z}} = -\eta_0 b_2 \frac{2}{3}\frac{\left(\frac{1}{\mathcal{Z}} + \frac{2}{5} + \frac{3}{5}X\right)^2}{1-X}, \quad (23b)$$

$$\frac{\eta_{11}^{(K)}}{\rho\mathcal{Z}} = \eta_0 b_2 \frac{4}{3}\frac{\left(\frac{1}{\mathcal{Z}} + \frac{2}{5} + \frac{3}{5}X\right)^2}{1-X}, \quad (23c)$$

$$\frac{\eta_{B}^{(K)}}{\rho\mathcal{Z}} = \frac{1}{3}\left(\eta_{11}^{(K)} + 2\eta_{12}^{(K)}\right) = 0, \quad (23d)$$

and for the α parts there are

$$\frac{\eta_{44}^{(\alpha)}}{\rho\mathcal{Z}} = \mathcal{E}_1\mathcal{F}_1, \quad (24a)$$

$$\frac{\eta_{12}^{(\alpha)}}{\rho\mathcal{Z}} = \mathcal{E}_2\mathcal{F}_2 - \mathcal{E}_3\mathcal{F}_3, \quad (24b)$$

$$\frac{\eta_{11}^{(\alpha)}}{\rho\mathcal{Z}} = \mathcal{E}_2\mathcal{F}_2 + 2\mathcal{E}_3\mathcal{F}_3, \quad (24c)$$

$$\frac{\eta_{B}^{(\alpha)}}{\rho\mathcal{Z}} = \mathcal{E}_2\mathcal{F}_2. \quad (24d)$$

The expressions presented above are used to obtain the RET results for TC in the Section IV C.

IV. RESULTS AND DISCUSSION

In this section the main results for the hard sphere fluid and solid are presented. This section also focuses on the assessment of the accuracy of the Revised Enskog Theory by comparison with the 'exact' MD quantity values. First the fluid phase is considered.

A. FLUID

In this work the equation of state, $\mathcal{Z}$, is considered to be a known function of density and given by the mKLM formula for the fluid and the S2 formula for the solid from our previous studies [22].

In this section the results of an analysis of the transport coefficients of the HS fluid are presented. This region has been the subject of a number of intensive investigations in the past [22, 27, 29, 33–37]. Here some viscosities are reported at state points not given previously. Also the different parts of the TC are presented separately, including the instantaneous contribution. All three components of the viscosity tensor are determined in order to compare with those for the solid, and to consider the different bulk viscosity formulations. These data are given in Tables IV - VIII in Appendix A. Some of the total η_S and λ values were given in our previous studies [22, 27] and are included here for completeness, together with their kk, kc, cc, and I separated contributions which were not always presented in those original publications.

In Figs. 1 - 2 the total, and kk, kc, cc and I parts of the viscosities and thermal conductivity are presented, and show a number of already known types of behavior. For example, the low density region is dominated by the kk part and the dense region by the cc part in all cases. The low density limiting values agree with those from kinetic theory [2]. In the freezing region the cc part increases considerably with density and the kk part becomes negligible. The bulk viscosity originates from the cc part only.

As all parts of η_L, η_S and η_B are non-negative it follows from the definition in Eq. (4) that the kk, kc parts of η_{12} must be negative in a HS fluid below a certain density. Consequently in the low density region dominated by the kk part the cross viscosity η_{12} is negative below $\rho \sim 0.44$ (see Fig. 1b). Additionally, due to the fact that $\eta_B^{kk} = \eta_B^{kc} = 0$ a number of relations for the kk and kc parts are met, i.e., $\eta_L^{kk} = -2\eta_{12}^{kk}$, $\eta_S^{kk} = -3\eta_{12}^{kk}/2$, $\eta_L^{kk} = 4\eta_S^{kk}/3$, $\eta_L^{kc} = -2\eta_{12}^{kc}$, $\eta_S^{kc} = -3\eta_{12}^{kc}/2$ and $\eta_L^{kc} = 4\eta_S^{kc}/3$. All these relations are seen to be obeyed well in the data presented in Fig. 1 and Tables IV - VIII, and are fulfilled by the Enskog relations below. These relations can be considered to be a useful cross check for the viscosity calculations.

For the single component HS fluid the RET theory gives the same expressions as Enskog theory (compare Eqs. (7)-(9) and (22)-(24) with $F' = 0$ or $X = 0$, and
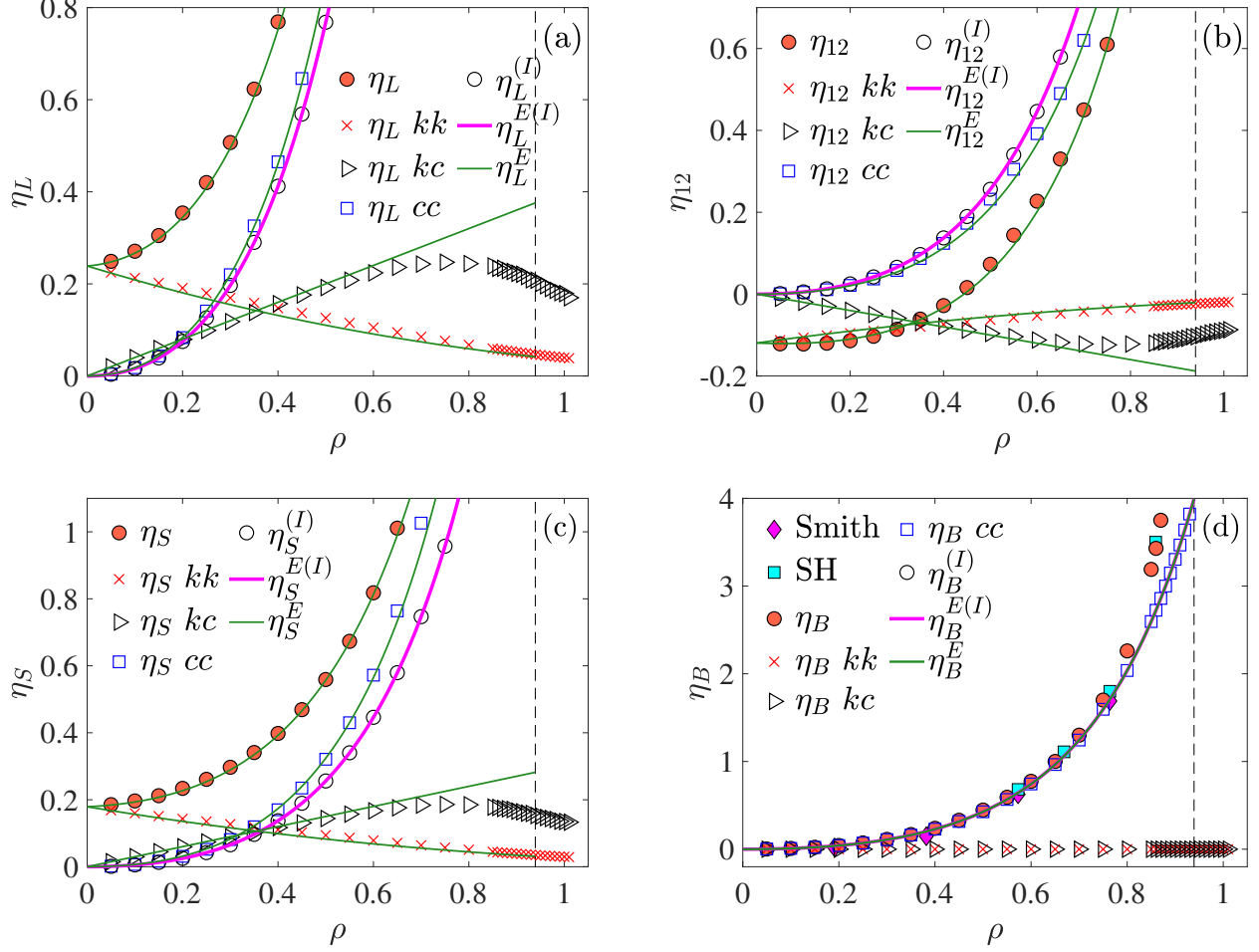
FIG. 1. The values of the transport coefficients (a) η_L, (b) η_{12}, (c) η_S and (d) η_B, and their components (kk, kc, cc, I) are shown as a function of density for the HS fluid and in its metastable fluid region. The red solid circles are the total MD transport coefficient values of this work (see Tables IV - VIII in Appendix A). All of the sets of data are values obtained by extrapolation to the thermodynamic limit. The red crosses, black right-triangles and blue open squares are the kk, kc, cc components of the viscosities, respectively. The open black circles are the instantaneous (singular) part of the presented transport coefficients, calculated from MD. In frame (d) the acronym 'Smith' refers to data from Ref. 32 and 'SH' from Ref. 29. The solid green lines are the Enskog formulas from Eqs. (25) for the total and kk, kc, cc components. The solid magenta line is the instantaneous (singular) part of Enskog prediction. The vertical thin dashed line indicates the freezing density, $\rho_{fr} = 0.9392$.

$\eta_3 = 0$) and the corresponding expressions are [2, 36],

$$\eta_S^E = \eta_{00} \frac{b_2 \rho}{\mathcal{Z}} \left[1.016 \left(1 + \frac{2}{5}\mathcal{Z} \right)^2 + \frac{48}{25\pi}\mathcal{Z}^2 \right]$$

$$= \eta_{00} \frac{b_2 \rho}{\mathcal{Z}} \left[1.016 + 0.8128\mathcal{Z} + 0.7737\mathcal{Z}^2 \right], \text{(25a)}$$

$$\eta_{12}^E = -\eta_{00} \frac{b_2 \rho}{\mathcal{Z}} \left[1.016 \frac{2}{3} \left(1 + \frac{2}{5}\mathcal{Z} \right)^2 - \frac{48}{25\pi}\mathcal{Z}^2 \right]$$

$$= -\eta_{00} \frac{b_2 \rho}{\mathcal{Z}} \left[0.6773 + 0.5419\mathcal{Z} - 0.5028\mathcal{Z}^2 \right] \text{(25b)}$$

$$\eta_L^E = \eta_{00} \frac{b_2 \rho}{\mathcal{Z}} \left[1.016 \frac{4}{3} \left(1 + \frac{2}{5}\mathcal{Z} \right)^2 + \frac{144}{25\pi}\mathcal{Z}^2 \right]$$

$$= \eta_{00} \frac{b_2 \rho}{\mathcal{Z}} \left[1.3547 + 1.0837\mathcal{Z} + 2.0502\mathcal{Z}^2 \right], \text{(25c)}$$

$$\eta_B^E = \eta_{00} b_2 \rho \frac{16}{5\pi}\mathcal{Z}, \tag{25d}$$

$$\lambda^E = \lambda_{00} \frac{b_2 \rho}{\mathcal{Z}} \left[1.02522 \left(1 + \frac{3}{5}\mathcal{Z} \right)^2 + \frac{32}{25\pi}\mathcal{Z}^2 \right]$$

$$= \lambda_{00} \frac{b_2 \rho}{\mathcal{Z}} \left[1.02522 + 1.2303\mathcal{Z} + 0.7765\mathcal{Z}^2 \right] \text{(25e)}$$
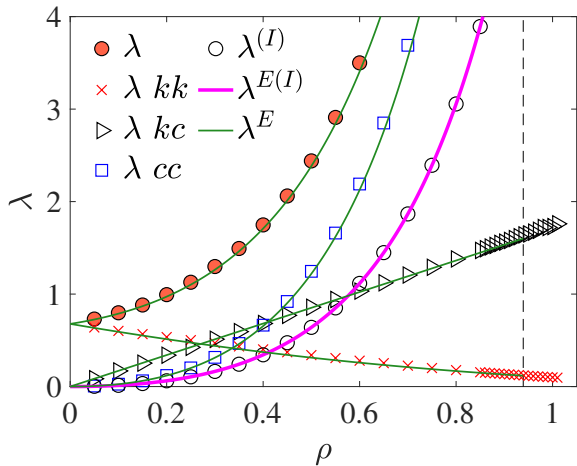
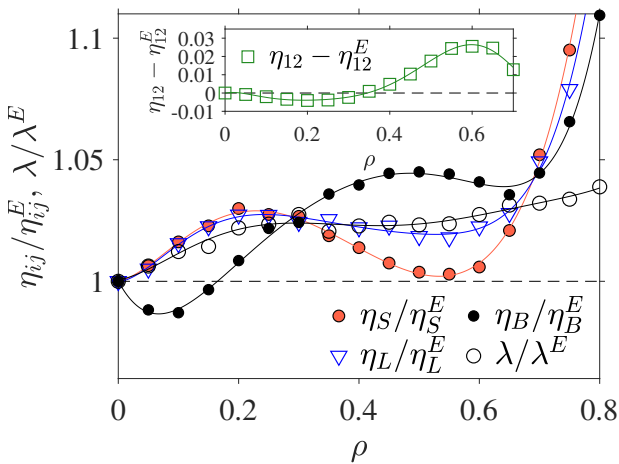FIG. 2. As for Fig. 1, except that in this instance the thermal conductivity, λ, is presented.

FIG. 3. The ratio of total η_{ij}/η_{ij}^E (for shear, longitudinal and bulk viscosities), and λ/λ^E for fluid states is presented. In the case of the cross viscosity the difference, $\eta_{12} - \eta_{12}^E$ rather than their ratio is shown in the inset. The Enskog formulas for viscosities and thermal conductivity are from Eqs. (25). The solid colored thin lines are only meant to guide the eye.

The two terms in the first line in the above equations represent the non-singular and instantaneous (singular) parts, respectively. In the second lines, the three terms represent the kinetic (kk), cross (kc) and collisional (cc) parts, respectively. In the case of the bulk viscosity in Eq. (25d) only the instantaneous part is present.

In Figs. 1 and 2 the computed values of different transport coefficients are compared with the Enskog theory predictions in Eqs. (25) (the solid green lines). Figure 3 shows that the agreement up to *ca.* 0.7 is very good in the cases of η_S, η_L, η_B while noticeable deviations become visible for these viscosities in the dense region. The behavior of η_{12} is different to the other viscosities
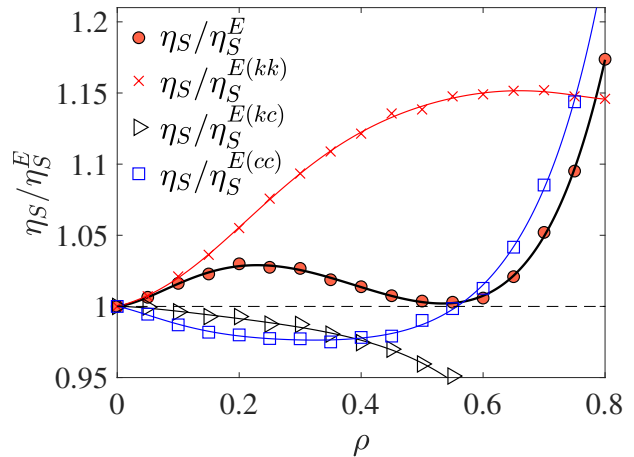

FIG. 4. The ratio η_S/η_S^E for the total value and individual kk, kc and cc terms are presented as a function of density for the fluid region. The Enskog formula for the shear viscosity is defined in Eq. (25a). The solid colored thin lines are only to guide the eye.

when compared with the Enskog formula values, in that a reasonable agreement is also observed for the dense fluid. Due to the sign change near 0.4, the difference, $\eta_{12} - \eta_{12}^E$, instead of the ratio, is presented in the inset of Fig. 3.

For λ the agreement is better than 5 % over the entire fluid phase. This is evident in figure 3 where the ratio TC/TC^E for the various transport coefficients and their Enskog predictions are shown.

It is noteworthy that in Fig. 3 and 4 there is a non-monotonic increase of this ratio for shear viscosity and where a small 'hump' at $\rho \approx 0.25$ is evident. There is a very good representation of this viscosity by the Enskog equation in the density range, $\rho \approx 0.5$ where $\eta_S \cong \eta^E$ is observed. This feature is a result of a competition between the kk and kc, cc parts (see Fig. 4) which means that a low order polynomial cannot be used to describe this behavior well.

All the calculated instantaneous parts made with the formulas in Eqs. (6) implemented in MD are in excellent agreement with the Enskog prediction for I-parts in Eqs. (25). This confirms that the Enskog predictions for $\eta_S^{(I)}$, $\eta_B^{(I)}$, $\eta_L^{(I)}$ and $\lambda^{(I)}$ are exact for all fluid densities as was shown in [17] and [11].

Furthermore, because for an isotropic system $\eta_3^{(I)} = 0$ the following relationship holds,

$$\eta_{11}^{(I)} - \eta_{12}^{(I)} - 2\eta_{44}^{(I)} = 0. \qquad (26)$$

This equation can be considered to serve as a simple indicator of the transition between isotropic and anisotropic phases, which may be a useful condition as the instantaneous parts are not computationally demanding to obtain and can be evaluated with considerable accuracy by MD.

TABLE II. The constants a_i, b_i used in linear representation of each TC for the solid as function of $\rho\mathcal{Z}$ in Eq. (27).

A_i	a_i	b_i
η_{11}	-0.1452	0.4266
η_{12}	0.0451	-0.1764
η_{44}	-0.0859	0.5058
η_B	-0.0046	0.0066
λ	-0.5012	1.8192

TABLE III. The constants a_i, b_i, and c_i used in the second-order polynomial representation of each TC for the solid as function of $\rho\mathcal{Z}$ which is given in Eq. (28).

A_i	a_i	b_i	c_i
η_{11}	0.5116	-1.4438	1.2470
η_{12}	0.2112	-0.4918	0.1634
η_{44}	-0.0767	0.1073	0.3846
η_B	0.0220	-0.0622	0.0440
λ	0.1155	-0.7841	1.9908

In the next two subsections IV B and IV C the HS solid state and its RET description are analyzed.

B. SOLID

The density dependence of the total, and kk, kc, cc parts of the transport coefficients η_{11}, η_{12}, η_{44}, η_B, and λ in the solid region are presented, in Figs. 5 - 6 and in Tables IV - VIII given in Appendix A. The figures show that for all TC in the solid phase only the cc part is significant, and the kk, kc components are negligible and are zero in the case of η_B. The η_{12} viscosity is negative over the entire solid phase. All transport coefficients diverge in the close packing (cp) limit apart from η_B which goes to zero. In the figures 5 - 6 the MD calculated instantaneous part is also presented, and as may be seen, for all the TC (including η_B) the I component monotonically increases strongly with density.

The assessment of the results simplifies considerably if the data are presented as the ratio $A_i/\rho\mathcal{Z}$, where A_i stands for η_{11}, η_{12}, η_{44}, η_B or λ, and $i = 1, ..., 5$. As may be seen in Figs. 7 - 8 this ratio can be approximated well by the simple linear function of the form, $a_i\rho + b_i$, where the constants, a_i and b_i are given for each TC in Table II. Therefore, to a good approximation, in the solid all the TC are well represented by the form $(a\rho + b)\rho\mathcal{Z}$. If it is further observed that $1/\mathcal{Z}$ is represented well by the linear formula $\approx 0.2547(\rho_{cp} - \rho)$ (a similar feature was noted for the dense fluid branch by Le Fevre [38]) an explicit approximate generic density dependent formula for the solid HS transport coefficients is,

$$A_i \approx (a_i\rho + b_i)\rho\mathcal{Z} \approx (a_i\rho + b_i)\frac{3.93\rho}{\rho_{cp} - \rho}. \qquad (27)$$

The existence of such a simple and at the same time relatively accurate representation of the TC in the HS solid we consider to be a significant result. This observation could facilitate the discovery of interrelationships between different TC, which have been the subject of a number of previous theoretical studies of fluids [34, 35]. For example, the ratio, η_{44}/η_{12} is approximately constant because the magnitude of the parameter a_i (or slope with density) for both quantities is small. From the above formula in Eq. (27) it may be concluded that the asymptotic behavior of $A_i(\rho \to \rho_{cp})$ follows that of $\mathcal{Z}$ and is the same for all of the transport coefficients.

Almost perfect agreement can be obtained, even close to melting, by replacing the above linear approximation by a second-order polynomial,

$$A_i \approx (a_i\rho^2 + b_i\rho + c_i)\rho\mathcal{Z}, \qquad (28)$$

where the values of a_i, b_i, and c_i are given for each TC in Table III. As the TC of the solid is represented almost entirely by the cc part, the above approximate description is to a large extent a description of the cc part.

In the case of the I part of the TC, several features may be identified. For each A_i the I part is always positive and becomes a quite relevant contribution on increasing density. As already mentioned, in the fluid the calculated values follow exactly from the I parts of the formulas in Eqs. (25) which is visible as the magenta dots forming horizontal lines in the graphs in Figs. 7 and 8. For λ and η_B the horizontal line is exactly continued from the fluid into the solid phase, until $\rho \to \rho_{cp}$ without any change in the transition region. This indicates that Eqs. (6) describe the I part of the HS system over the entire density range of the system. The situation is different for the I parts of the other three TC (η_{11}, η_{12}, and η_{44}). As may be seen in Fig. 7 there is a jump or discontinuity which takes place in the freezing-to-melting metastable transition region. The difference $\Delta_i = A_i^{(I)}(\rho_f)/\rho_f\mathcal{Z} - A_i^{(I)}(\rho_m)/\rho_m\mathcal{Z}$ (where ρ_f and ρ_m are the freezing and melting densities, respectively) is positive in the case of η_{11} and negative for η_{12} and η_{44}. Moreover, the jump is the same for the shear and cross parts, i.e., $\Delta_2 \cong \Delta_3$, and $\Delta_1 \cong -2\Delta_3$. Also, the density dependence of the equation of state-scaled I part of TC, in the solid phase, can be approximated well by a straight line with a slight nonzero slope. These features of the I part will be discussed within the context of the RET in the next subsection IV C.

C. RET

Instantaneous and kinetic part of the TC

The importance of the quantity, F', is that it allows us to obtain the kinetic contribution to the RET viscosities and thermal conductivity from Eqs. (9) and (23). Also, in the case of the thermal conductivity knowledge of F',
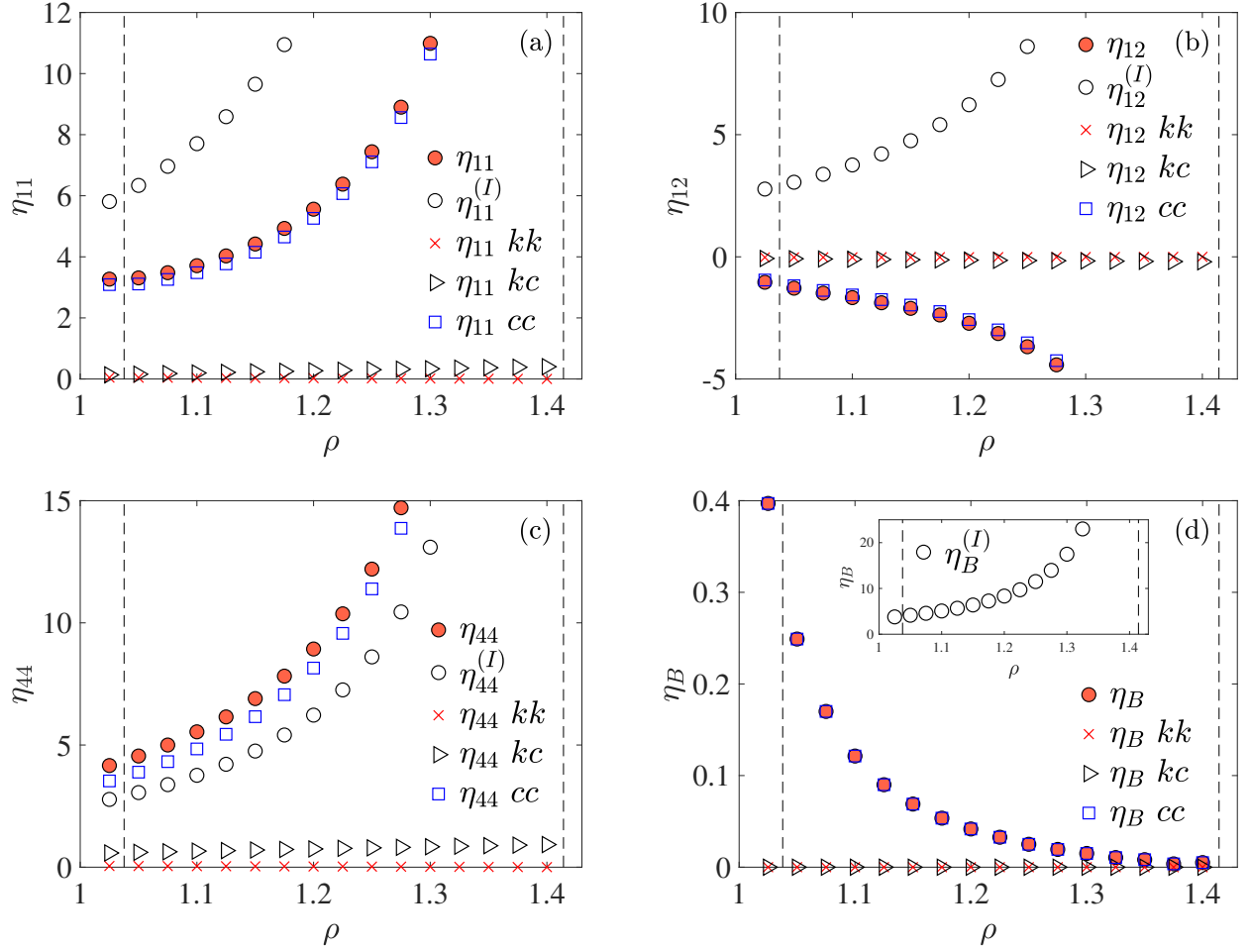
FIG. 5. The values of the hard sphere solid transport coefficients (a) η_{11}, (b) η_{12}, (c) η_{44}, (d) η_B and their components (kk, kc, cc and I) are shown as a function of density. The red solid circles are the MD results (total value) of this work (see Tables IV - VIII in Appendix A). All of the sets of data were obtained by extrapolating the $N-$ dependent MD data to the thermodynamic limit. The red crosses, black right-triangles and blue squares are the kk, kc, cc components of viscosities, respectively. The open black circles are the instantaneous (singular) part of the presented transport coefficients (from MD). The vertical thin dashed lines indicate from the left the melting ($\rho_m = 1.0376$) and close packing ($\rho_{cp} = \sqrt{2}$) densities.

allows us to determine $\lambda^{RET} = \lambda^{(I)} + \lambda^{(K)}$, and therefore to assess the relationship, $\lambda^{(Q)} = \lambda - \lambda^{RET}$, and hence the RET prediction of the thermal conductivity.

Thus, the function F' is a key quantity for the RET treatment and it was calculated directly from its definition in Eq. (10) and also from the I part of the viscosities in Eqs. (14). In the first case, the calculations consisted of building a two-dimensional histogram (or surface) of the collisions of molecules. In the solid, each collision was described in spherical coordinates by two angles. The F' function is the integral of the histogram surface for each density. The results of these calculations are given in Fig. 9a, where the function $X = F'/\mathcal{Z}$ is presented. As is visible in the figure the values of X obtained by the three approaches specified in the caption (presented as solid black point, black crosses and red pluses) are in good mutual agreement. This

is an important result as Fig. 9a indicates that, just as for the Enskog expressions for the fluid, the RET formulas describe exactly the I part of the TC in the solid. Consequently, the behavior of the I part obtained from MD in Figs. 7 and 8 can be explained with the RET expressions in Eqs. (7) and (22). This includes the observed jumps at the freezing-melting transition which are $\Delta_2 = \Delta_3 = -\Delta_1/2 \cong 0.2222X(\rho_m) \cong -0.0499$.

The X function is negative and weakly density dependent and decreases to -0.25 in the close packing limit. The characteristic extrapolated value, $X(\rho_{cp}) = -0.25$ can also be inferred by heuristic considerations which are given in Appendix B. With the known F' or X and Eqs. (9) and (23), the kinetic part of the RET contributions to all TC can be obtained, and they are shown (as green dots) in Figs. 7 - 8. The K parts divided by $\rho\mathcal{Z}$ can be seen to be well represented by a straight line for all the
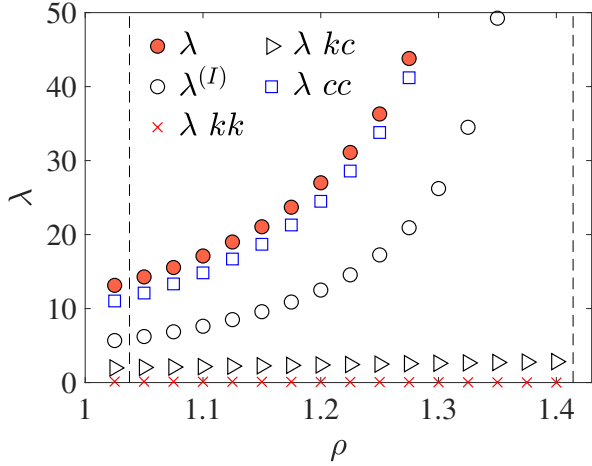
FIG. 6. As for Fig. 5, except that the thermal conductivity, λ, data are presented.

TC.

For λ, there are at least two points to observe in Fig. 8: a) the K part is larger than the I part and both contributions become almost equal at close packing, b) the $\lambda^{(Q)}$ contribution is very small and almost constant (i.e., it only very slightly decreases with rising density) and is negative. The agreement with the simulation data is within 2% over the entire solid phase, and it may be concluded that in the solid phase the RET describes the thermal conductivity almost exactly. In Ref. 27, the relation $\lambda = \lambda^{RET}$ (i.e., $\lambda^{(Q)} = 0$) was taken as an assumption which led to two solutions for $X(\rho)$ which represent this quantity well over the entire density range, and has an almost constant value, i.e., $X \approx 0.2$ and -0.2 (in approximation both solutions yield the same value of λ^{RET}). As is shown in this work the values of X and F' are negative, and $\lambda^{(Q)}$ is very small, which makes the assumption made in Ref. 27 quite plausible and justified.

In the case of the viscosities, as seen in Fig. 7, the K part is lower in magnitude than the I part. The viscosity components, $\eta_{11}^{(K)}$ and $\eta_{12}^{(K)}$ are weakly density dependent and quite small (no larger than 20 % of the total value of η_{11} and η_{12} near melting). The calculation of the kinetic contribution to the bulk viscosity leads to the conclusion that $\eta_B^{(K)}$ is exactly zero, just as for the fluid. This means that the sum $\eta_B^{(Q)} + \eta_B^{(\alpha)}$ is negative and well-represented by $-\eta_B^{(I)} = -(\eta_{11}^{(I)} + 2\eta_{12}^{(I)})/3$. Only in the case of the shear viscosity is the K contribution substantial (and about 37% of η_S).

In regard to the viscosity tensor, unlike for λ, knowledge of the I and K parts is not sufficient to assess the performance of the RET, some knowledge of the $\eta_{ij}^{(\alpha)}$ part is also necessary.

α-part of the TC

This third part of the p-viscosities is much more demanding to assess than the other contributions. As described in Eq. (24) of Sec. III the $\eta_{ij}^{(\alpha)}$ part can be expressed as the product of $\rho\mathcal{Z}$ and the elastic $\mathcal{E}_p$ and dissipative $\mathcal{F}_p$ terms.

The $\mathcal{F}_p$ terms in $\eta^{(\alpha)}$

To obtain the $\mathcal{F}_p$ term, evaluations of the $\bar{\mathcal{Z}}$ and $\bar{F}'$ functions in Eqs. (20) and (21) were carried out in the same way as for calculations of F' in Eq. (10). The $\bar{\mathcal{Z}}$ quantity is a strongly increasing function with density and $\bar{F}'$ is negative and a strongly decreasing one. Both vary as $\sim 1/\alpha$ (where α is the dimensionless width of the one-particle density distribution) as was indicated in Ref. 8. The resultant ratios, $\bar{X}$ and W together with X are given as a function of density in Fig. 9a. In the figure we observe that X and $\bar{X}$ are very similar over the density entire range although the functions F', $\bar{F}'$, Z and $\bar{Z}$ differ significantly from each other. Also, the considerations as for the X in the Appendix B, give the same limiting value $\bar{X}(\rho_{cp}) = -0.25$.

A noteworthy result seen in Fig. 9a is the quasi-linear behavior of αW in particular its zero value in the close packing limit. This is mainly due to the almost linear density dependence of $1/\mathcal{Z}$ in the solid and that $\alpha\bar{\mathcal{Z}}$ is small and weakly density dependent. Consequently Fig. 9b demonstrates that all of the $\alpha\mathcal{F}_p$ terms display an almost linear dependence with density and become exactly zero at close packing. This trend indicates that at densities near to close packing the contribution of $\eta_{ij}^{(\alpha)}$ might be negligible. Also, due to the fact that $X(\rho) \cong \bar{X}(\rho)$ and that $X(\rho)$ has an almost constant value, the expressions in Eqs. (18) can be represented well by the following simplified forms,

$$\mathcal{F}_1 = \eta_{00}\frac{16}{5}\left(\frac{1}{5}(1-X) - \frac{\pi}{16}\left(\frac{1}{\mathcal{Z}} + \frac{2}{5}(1-X)\right)\right)W$$
$$\cong (0.03395\rho + 0.03847)W, \tag{29a}$$

$$\mathcal{F}_2 = \eta_{00}\frac{16}{15}W = 0.18806W, \tag{29b}$$

$$\mathcal{F}_3 = \eta_{00}\frac{16}{15}\left(\left(\frac{2}{5} + \frac{3}{5}X\right) - \frac{\pi}{8}\left(\frac{1}{\mathcal{Z}} + \frac{2}{5} + \frac{3}{5}X\right)\right)W$$
$$\cong (0.01516\rho + 0.00670)W. \tag{29c}$$

Consequently the following approximate relations hold, $\mathcal{F}_1 \approx \frac{2}{5}\mathcal{F}_2 \approx 4\mathcal{F}_3 \approx \eta_{00}(32/75)W = 0.0752W$.

As mentioned above (see Eqs. (24)) the $\eta_{ij}^{(\alpha)}$ part divided by $\rho\mathcal{Z}$ is a product of the $\mathcal{F}_p$ term and the elastic $\mathcal{E}_p$ term. Therefore, to obtain the contribution of this part, basically, both of these terms are necessary. As has been
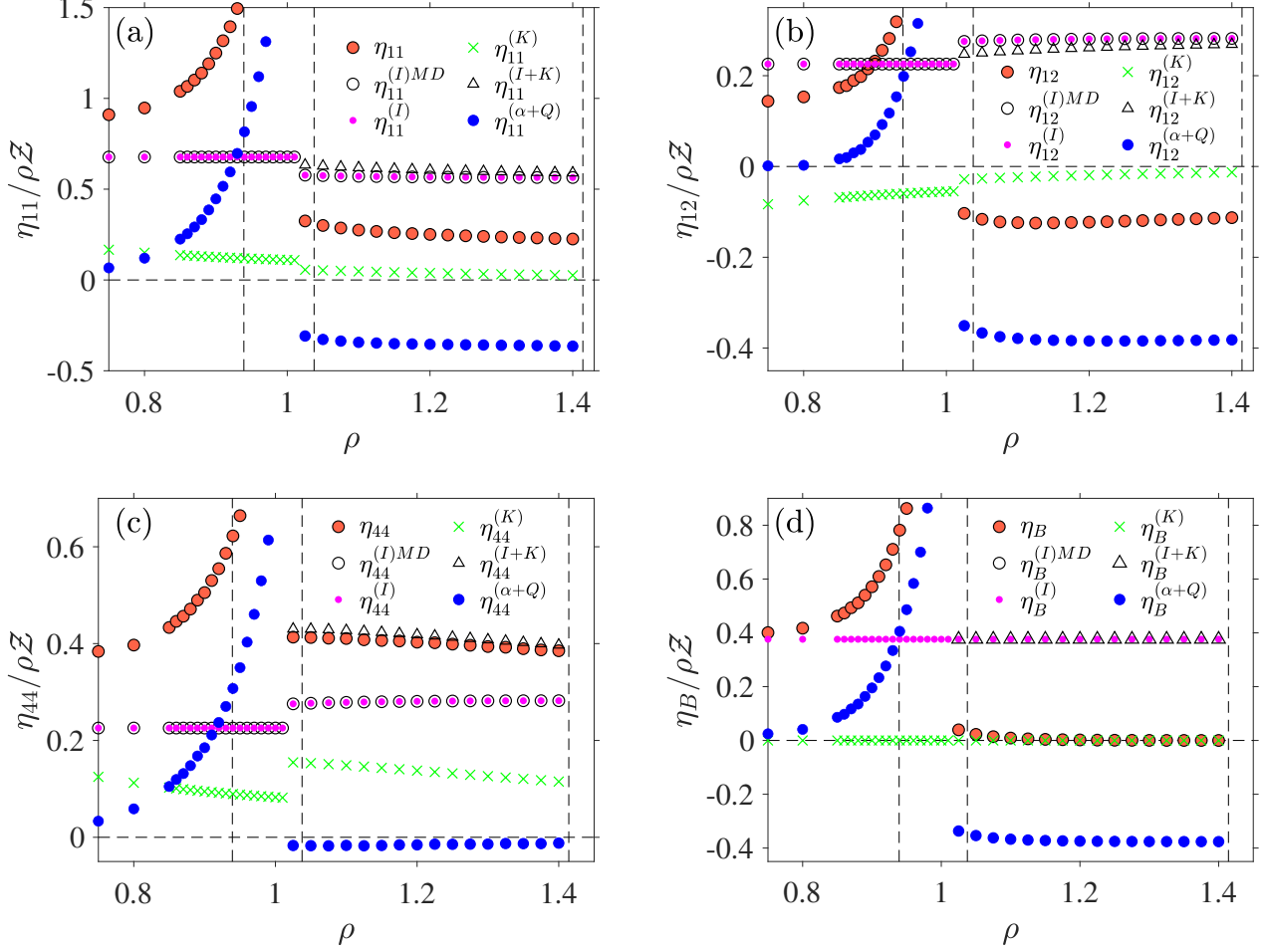
FIG. 7. The ratios: (a) $\eta_{11}/\rho\mathcal{Z}$, (b) $\eta_{12}/\rho\mathcal{Z}$, (c) $\eta_{44}/\rho\mathcal{Z}$, (d) $\eta_B/\rho\mathcal{Z}$ and its RET components (I, K, $\alpha + Q$) for hard spheres are shown as a function of density for the dense fluid and solid phase (including the fluid metastable and solid metastable regions). The red solid circles are the MD results (total value) of this work (see Tables IV - VIII in Appendix A). The open black circles are the MD data for the instantaneous part. All of the sets of MD data were extrapolated to the thermodynamic limit, whose values are presented on the figures. The magenta and green solid points are the I and K components of the viscosities in RET, respectively. The open triangles are the sum of these instantaneous and kinetic parts $(I + K)$ from RET. The blue solid points are the $(\alpha + Q)$ component obtained as $\eta_{ij} - \eta_{ij}^{(I+K)}$. The vertical thin dashed lines indicate from left the freezing ($\rho_{fr} = 0.9392$), melting ($\rho_m = 1.0376$) and close packing ($\rho_{cp} = \sqrt{2}$) densities.

shown in Fig. 9b, the $\alpha\mathcal{F}_p$ term is relatively small (the largest value is within 0.02 at the melting), decreases linearly with density and becomes practically zero at high densities.

The $\mathcal{E}_p$ terms in η^α

The elastic terms ($\mathcal{E}_p$) are functions of $C_{ij}^{\alpha u}$, $C_{ij}^{\alpha\alpha}$ i.e., the DFT components of the elastic modulus tensor, and their estimation is not straightforward. A possible approach is to evaluate these elastic terms with the approximate DFT model based on an expansion around reference liquid state [8, 30]. Such calculations were conducted previously (not only for the HS system) mainly

in order to locate the freezing-melting transition. As is known [30, 39] the DFT approach can provide only an approximate description of the elastic coefficients even if some higher order terms are included into the scheme [40]. Also, as the crystal density increases, the calculated DFT elastic components become increasingly less reliable and the calculated elastic constants deviate from the known values of the elastic HS constants (see Ref. 40). Also, it is physically reasonable to expect that because an expansion about the liquid is performed such an approach can be applied at solid densities not too far from melting.

The results obtained for the elastic terms using the approximate DFT approach are shown in Fig. 14 and the details of the calculations are given in Appendix C.
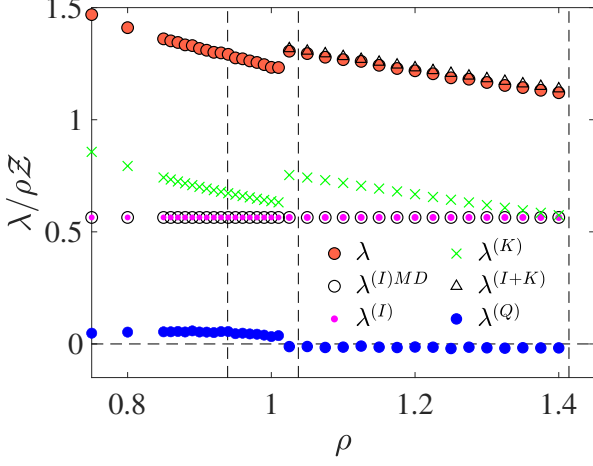
FIG. 8. As for Fig. 7, except that the thermal conductivity, $\lambda/\rho\mathcal{Z}$, data are presented.

The DFT calculations show that all elastic terms $\mathcal{E}_p$ are rather small in the density region considered. This gives the magnitude of $\mathcal{E}_p/\alpha$ to be of order 20 or less. Combining these results for elastic terms with the results obtained above for the $\mathcal{F}_p$ terms makes it possible to estimate the third α part of the RET viscosity tensor, which is shown in Fig. 10. These results indicate, that all viscosities (apart from the shear viscosity) may not be well described by the RET or that the $\eta_{ij}^{(Q)}$ part is relevant for them.

To summarize the situation, at moderate crystal densities which are not too far from the melting density, the order of magnitude estimates of the elastic components obtained from the DFT approximation can be considered to be reliable.

The question is, therefore, do the above conclusions remain valid for the more dense solid, in particular at densities close to ρ_{cp}? Note, because $\alpha\mathcal{F}_p$ goes to zero in the $\rho \rightarrow \rho_{cp}$ limit, the $\eta_{ij}^{(\alpha)}$ part should also go to zero if $\mathcal{E}_p/\alpha$ were to be bounded in this limit. Therefore, some estimation of the behavior of $\mathcal{E}_p/\alpha$ at densities close to ρ_{cp} is desirable. The approach which may be helpful here, and not limited to the melting density region, is that mentioned above based on Appendix B in Ref. 8. This method requires calculations of so-called H-functions which are integrals involving the pair direct correlation functions (DCF) of the solid, $c(\mathbf{r}_1, \mathbf{r}_2)$. It should be appreciated that the DCF function is multidimensional and directionally-dependent, which is in practice a hardly accessible physical property. In general the evaluation of the DCF and consequently also the H-functions is a formidable task, and only recently have some calculations of the DCF of a hard sphere crystal been undertaken, which showed its appearance in some special cases [31, 41]. In that work, [31] it was demonstrated that the DCF of the crystal, like in the
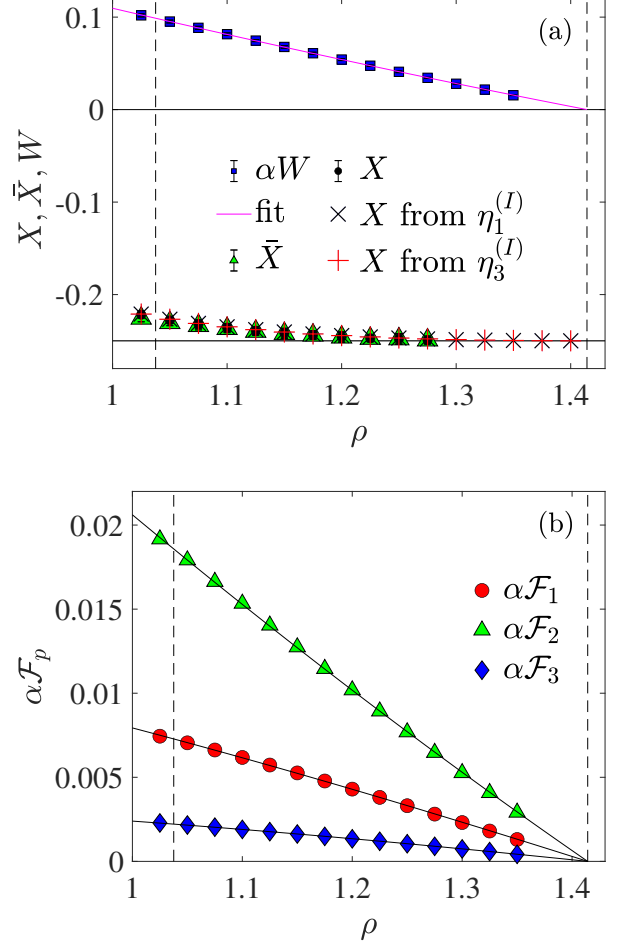
FIG. 9. In the top frame (a) the density dependence of the X, $\bar{X}$ and αW functions are presented. The blue solid squares, black solid points, green solid triangles are the values calculated directly from MD simulation (using the equation of state $\mathcal{Z}$, Eqs. (10), (21) and (20)). The black crosses and red pluses are the values obtained only from the instantaneous parts of MD data (using Eqs. (14a) and (14c)). The magenta line represents the fit, $\alpha W = 0.05949(\rho - \rho_{cp})^2 - 0.23993(\rho - \rho_{cp})$. In the bottom frame (b) the $\alpha\mathcal{F}_p$ vs ρ are shown. The points are the values calculated from the simulations (from Eqs. (18)), and the lines are obtained from the formulas in Eqs. (29). The vertical thin dashed lines indicate from the left to right, the melting ($\rho_m = 1.0376$) and close packing ($\rho_{cp} = \sqrt{2}$) densities.

fluid, is a short ranged function which goes quickly to zero for distances of about the size of the particle. This means that the contribution to the integrals defining the H-functions is negligible from distances larger than σ. It can also be inferred that for small distances the DCF function is almost linear or constant and to a large extent isotropic (and weakly depends on direction). At larger distances (but less than σ) the function is anisotropic, changes significantly with distance and presumably is also strongly density-dependent. Probably, for such

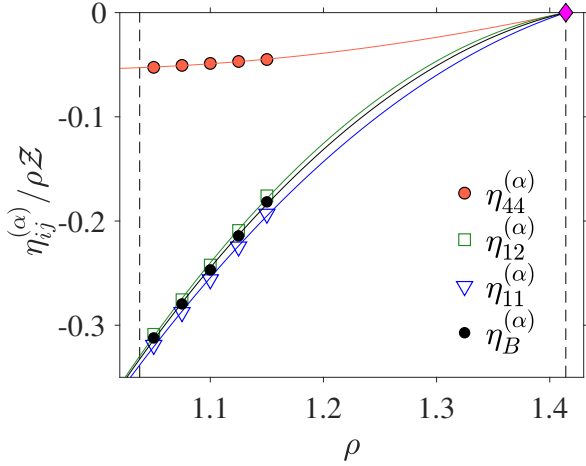FIG. 10. The ratios $\eta_{ij}^{(\alpha)}/\rho\mathcal{Z}$ estimated from the DFT approach, which are given by the colored solid points, are presented. The solid magenta diamond at the close packed density is the result estimated from the H integral approach given in Appendix D. The solid thin lines are the fits to the data. The vertical thin dashed lines indicate from left to right the melting ($\rho_m = 1.0376$) and close packing ($\rho_{cp} = \sqrt{2}$) densities.

distances no general behavior can be established.

Taking into account these established general features of the DCF and making some plausible assumptions about the relevant contributions to the integrals some estimation of the H-functions is possible, at least in the high density region. This procedure is followed in Appendix D where a simplified formula for the DCF is considered. The main conclusion is that $\mathcal{E}_p/\alpha$ is a bounded quantity or (like $\alpha\mathcal{F}_p$) even goes to zero in the $\rho \to \rho_{cp}$ limit. Consequently, the $\eta_{ij}^{(\alpha)}/\rho\mathcal{Z}$ part of the viscosities become negligible at high densities. This is consistent with the trend in the DFT results seen in Fig. 10.

RET assessment

Finally, having η_{ij}, the evaluated $\eta_{ij}^{(I)}$, $\eta_{ij}^{(K)}$ and estimated $\eta_{ij}^{(\alpha)}$ an assessment of the accuracy of RET is now possible. This is shown in Fig. 11, where the ratio $\eta_{ij}/\eta_{ij}^{RET}$ is given for shear, longitudinal and bulk viscosities, and λ/λ^{RET} is also shown. In the case of the cross viscosity, due to the sign change (which would result in division by zero), the inverse ratio $\eta_{12}^{RET}/\eta_{12}$ is shown. Several conclusions from Fig. 11 can be discerned. First, for practically the entire crystal region this ratio for λ and η_{44} is almost density independent, which contrasts starkly with their behavior in the fluid, where a considerable density dependence is observed for *ca.* $\rho > 0.7$. For densities $\rho < 0.7$ the transport coefficients in the fluid
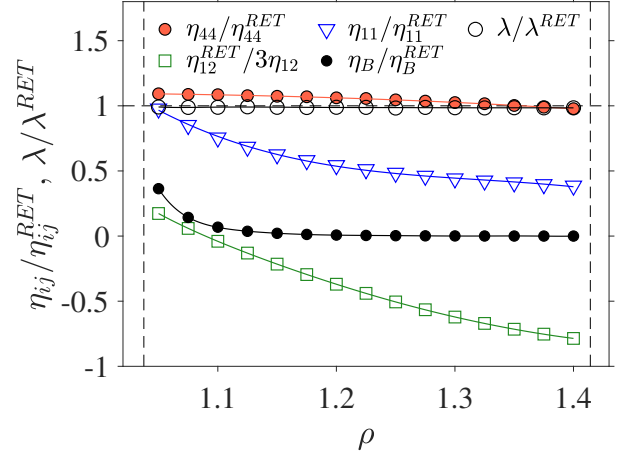

FIG. 11. The ratios, $\eta_{ij}/\eta_{ij}^{RET}$ and λ/λ^{RET} for the solid densities are presented. In the case of the cross viscosity the inverse ratio divided by 3 is shown. The solid colored lines are only meant to guide the eye. The vertical thin dashed lines indicate from the left the melting ($\rho_m = 1.0376$) and close packing ($\rho_{cp} = \sqrt{2}$) densities.

(as shown also previously in Fig. 3) are described well by the Enskog expressions given in Eqs. (25) with an accuracy better than 5%. In the solid the situation is different. The thermal conductivity and shear viscosity are represented well by the RET expressions covering the entire phase from melting to close packing density and in the case of the remaining three viscosities, η_{11}, η_{12} and η_B, we observe significant deviations from the RET predictions. A common feature of these viscosities is the smallness of the K part (which is zero in the case η_B, see Fig. 7d). Combining this observation with the negligibility of the α part at high densities, a simple relation is obtained for these three viscosities i.e., $\eta \cong \eta^I + \eta^Q$ for the dense HS crystal. We also note that in the case of the bulk viscosity the relation $\eta^Q \cong -\eta^I$ is well obeyed not only for $\rho \to \rho_{cp}$ but for most of the solid phase.

V. SUMMARY AND CONCLUDING REMARKS

In this work a comprehensive study of the viscosity tensor components and thermal conductivity of the HS system in both fluid and solid phases has been performed. The transport properties and their component parts were determined by MD simulations to an extent and accuracy not reported previously in the literature. The results for the crystal are largely new and display, unlike in the fluid, a surprisingly simple behavior e.g., all transport coefficients considered can be represented well by a simple function of density multiplied by the factor $\rho\mathcal{Z}$, as given in Eq. (27).

The instantaneous part of the transport coefficients have been evaluated directly by molecular dynamics simulations and compared with the kinetic theory (Enskog

and RET) predictions demonstrating their total mutual agreement, implying that short time dynamics in RET is exact [5, 8].

The (total) cross viscosity exhibits a different behavior to the other viscosities, in being negative in the entire solid phase and changes sign on increasing the density in the fluid phase (from negative to positive). Its negative value in the fluid results from the dominant role of the negative kk part in the dilute region. In the solid the behavior of the transport coefficients is determined almost completely by their cc part and the negative value results from a competition between the positive instantaneous I part, which is the contribution from the first collision in the Einstein-Kubo-Helfand formula, and a negative Q part, which represents all contributions not included in the RET formulation.

In contrast to the other transport coefficients, values of the bulk viscosity in the solid are quite small and decrease rapidly on increasing density, and go to zero in the close packing limit. Thus, an almost perfect cancellation between η_{11} and $2\eta_{12}$ exists in the HS crystal.

The observed perfect representation of the shear viscosity by the Enskog formula at moderate fluid densities (close to $\rho \approx 0.5$) is rather accidental, caused by the density dependence of the kk, kc, cc parts.

The results obtained for the transport coefficients of the HS system allowed us to review the performance of the RET description of the solid phase. To do such an analysis all parts of the RET expressions for the TC were determined i.e. I, K for λ and I, K, α for the viscosities. The α (the most complex) part has been estimated to an extent which enables this examination to be carried out effectively. Its dissipation term was calculated accurately and the elastic term was estimated with an approximate DFT approach, and from the H-functions method applied to the high density limit. In the case of the thermal conductivity the agreement between 'exact' MD and predicted RET results is excellent, better than 2% over the entire crystal phase. The prediction is better than for the fluid, which is itself known to be very good. Similarly the agreement is quite good in the case of the shear viscosity (i.e., η_{44}). In these cases the dynamic effects not included in the kinetic theory are negligible or mutually cancel out, making their contributions $\lambda^{(Q)}$, $\eta_{44}^{(Q)}$ very small.

In the case of the other viscosities the agreement is not so good, predictions of the RET differ considerably from the simulation results. For η_{11}, η_{12} and η_B the corresponding Q parts are substantial.

A summary of the performance of the kinetic theory predictions is shown in Fig. 11. The noteworthy feature of this figure is the almost constant (or density independent) behavior of the presented ratios for λ and η_{44} in the solid phase. Also, in the case of the bulk viscosity an unexpected and very simple description of the complex dynamic contribution not included in RET, i.e., $\eta^{(Q)} \cong -\eta^{(I)}$ is found for almost the entire solid phase.

The performed studies of the α part indicate that more results for its elastic term are required and that this may be achieved with the H-function approach along with the recently proposed DCF calculations.

The RET kinetic theory method like the original Enskog formulation is based on a solution of the classical dynamics of individual particles, albeit with assumptions about correlations (or lack thereof) between successive collisions. A relatively unambiguous comparison can then be made with explicit particle-based MD simulations. Nevertheless, it is worth exploring other alternative approaches which could potentially be used to model the behavior of the system properties covered in this work. For example, a stochastic mean-field differential equation time stepping meth-od has recently been developed which is not based on kinetic theory, [42], and has been applied to hard sphere liquids in infinite dimension. This method shows promise for highly viscous systems, and it would be interesting to discover if it could be extended to apply to solids in which the particles have anisotropic spatial correlations.

The additional characterization and understanding obtained in this work on hard sphere fluid and solid transport coefficients can be useful in general for the development of microscopic theories of transport properties in condensed matter. In particular, the present results may contribute to a further development of the RET approach for the current mono component hard sphere system and for other dense systems e.g., binary HS mixtures for which I, K parts may be sufficient to determine the thermal conductivity. It would be interesting to investigate if some aspects of the residual or Q-part could be included in a revised RET formulation, as this term has been shown to contribute significantly to the viscosity components (for example, including the effects due to correlations between successive particle collisions at a mean field level). Also this work provides a considerable body of new hard sphere data for this key reference system. The work fills a gap in the numerical determination and understanding of the transport properties of one of the most investigated model systems in condensed matter physics.

Appendix A: MD data and size dependence

The MD data indicate that the system size dependence of the all viscosities considered (including their kk, kc, cc and I parts) can be represented well by the following expression $\eta_{ij}^{(\infty)} = \eta_{ij}^{(N)} + \mathcal{A}_{ij}/N$, where $\mathcal{A}_{ij}$ is a positive constant at a given density. In the case of the thermal conductivity the N-dependence is different [27]. A detailed study indicates that $\lambda^{(\infty)} = \lambda^{(N)} + \mathcal{B}/N^{2/3}$, while its instantaneous part is represented by $\lambda^{(\infty)} = \lambda^{(N)} + \mathcal{B}^*/N$. Here $\mathcal{B}$ and $\mathcal{B}^*$ also are positive density dependent constants. In this work the identities, $\eta_{ij} \equiv \eta_{ij}^{(\infty)}$ and $\lambda \equiv \lambda^{(\infty)}$, are employed.

The N-dependence for two selected transport coefficients (η_{11} and λ) is shown in Fig. 12 for the instantaneous part and in Fig. 13 for the total value of them. Data for a fluid (at $\rho = 0.4$) and a solid (at $\rho = 1.1$) state points are presented. Other viscosities considered in this work show a similar N-dependence to that of the longitudinal viscosity.

The total values of the TC and their kk, kc, cc and I part in the thermodynamic limit are collected in the Tables IV - VIII and Supplemental Material [43] for the fluid and solid phases.

Appendix B: F' function in the limit of the close packing

In this appendix the close packing limiting value of the F' function is considered. Note that its definition in Eq. (10) can be written as follows:

$$F' = \int d\hat{\sigma}(5\hat{\sigma}_x^4)\Phi(\hat{\sigma}) - \int d\hat{\sigma}\Phi(\hat{\sigma}), \qquad \text{(B1)}$$

where

$$\Phi(\hat{\sigma}) = \frac{\sigma^3}{4\rho V} \int d\mathbf{r}_1 \varrho(\mathbf{r}_1)\varrho(\mathbf{r}_1-\sigma\hat{\sigma})G_2(\mathbf{r}_1,\mathbf{r}_1-\sigma\hat{\sigma}), \quad \text{(B2)}$$

and in terms of $\Phi(\hat{\sigma})$,

$$\mathcal{Z} = \frac{2}{3} \int d\hat{\sigma}\,\Phi(\hat{\sigma}). \qquad \text{(B3)}$$

In the close packing limit the contribution to the integral over $d\hat{\sigma}$ comes basically from the 12 directions on which nearest neighbors (nn) HS particles are placed in the fcc lattice. For the four nn in the yz plane, $\sigma_x = 0$ and for the remaining eight nn, $\sigma_x = \sqrt{2}/2$. This means that in this limit the first term in Eq. (B1) is $8 \cdot 5 \cdot (\sqrt{2}/2)^4/12 = 5/6$ of the second term, which gives

$$F' = \left(\frac{5}{6}-1\right) \int d\hat{\sigma}\,\Phi(\hat{\sigma}) = -\frac{\mathcal{Z}}{4}, \qquad \text{(B4)}$$

or $X(\rho_{cp}) = F'/\mathcal{Z} = -0.25$.

Appendix C: Estimation of the elastic terms at moderate crystal densities from the DFT method

In the calculations of the elastic terms the DFT method described in Refs. 30, 40, and 44 is used. The following formulas are exploited for these calculations,

$$\tilde{C}_{11}^{\epsilon\alpha} = -\frac{\eta+1}{2\alpha} - \frac{a^2}{4}\rho_L \sum_{\{\mathbf{G}\}} \xi_G^2 \frac{c_L^{'(2)}(|\mathbf{G}|)}{|\mathbf{G}|}G_1^4, \text{(C1a)}$$

$$\tilde{C}_{11}^{\alpha\alpha} = \frac{\eta+1}{2\alpha^2} - \frac{a^4}{8}\rho_L \sum_{\{\mathbf{G}\}} \xi_G^2 c_L^{(2)}(|\mathbf{G}|)G_1^4, \quad \text{(C1b)}$$

$$\tilde{C}_{12}^{\epsilon\alpha} = -\frac{\eta+1}{2\alpha} - \frac{a^2}{4}\rho_L \sum_{\{\mathbf{G}\}} \xi_G^2 \frac{c_L^{'(2)}(|\mathbf{G}|)}{|\mathbf{G}|}G_1^2 G_2^2 \text{(C1c)}$$

$$\tilde{C}_{12}^{\alpha\alpha} = -\frac{a^4}{8}\rho_L \sum_{\{\mathbf{G}\}} \xi_G^2 c_L^{(2)}(|\mathbf{G}|)G_1^2 G_2^2, \quad \text{(C1d)}$$

$$\tilde{C}_{44}^{\epsilon\alpha} = -\frac{a^2}{4}\rho_L \sum_{\{\mathbf{G}\}} \xi_G^2 \frac{c_L^{'(2)}(|\mathbf{G}|)}{|\mathbf{G}|}G_1^2 G_2^2, \quad \text{(C1e)}$$

$$\tilde{C}_{44}^{\alpha\alpha} = \frac{\eta+1}{4\alpha^2} - \frac{a^4}{8}\rho_L \sum_{\{\mathbf{G}\}} \xi_G^2 c_L^{(2)}(|\mathbf{G}|)G_1^2 G_2^2, \text{(C1f)}$$

where ρ_L is the density of the reference liquid, α describes the dimensionless width of the one-particle density distribution, a is the real space lattice-constant parameter (from which the solid density, ρ_S, can be obtained) and $\eta = (\rho_S - \rho_L)/\rho_L$. In the above equations $\mathbf{G}$ is the set of reciprocal lattice vectors, $c_L^{(2)}(|\mathbf{G}|)$ is the liquid pair direct correlation function (DCF) and $c_L^{'(2)}(|\mathbf{G}|)$, $c_L^{''(2)}(|\mathbf{G}|)$ are their first and second derivatives, respectively. The DCF and their derivatives were calculated analytically from the Percus-Yevick approximation.

In the Eqs. (C1) the quantity,

$$\xi_G = (\eta+1)\exp\left(-\frac{1}{4}|\mathbf{G}|^2 a^2\alpha\right), \qquad \text{(C2)}$$

is included, which is a Fourier transform of the one-particle density distribution (represented by the Gaussian distribution).

In the presented DFT method the isothermal elastic moduli are computed by minimizing the grand thermodynamic potential of the unstrained solid [40, 44], with respect to the density of the reference liquid ρ_L, the equilibrium width α and the lattice-constant parameter a. As demonstrated in Ref. 40 it is necessary in these calculations to take a very large number of reciprocal wave

TABLE IV. Longitudinal viscosity, η_{11}, and its components from MD computations as a function of density for fluid and solid phase (in units of $\sigma^{-2}(mk_BT)^{1/2}$)

ρ	η_{11}	η_{11}^{kk}	η_{11}^{kc}	η_{11}^{cc}	$\eta_{11}^{(I)}$
0.050	0.249(1)	0.2250(7)	0.0200(1)	0.00419(1)	0.003788(1)
0.100	0.271(1)	0.2128(9)	0.0398(2)	0.01791(4)	0.016231(1)
0.150	0.305(1)	0.2020(9)	0.0597(5)	0.0434(2)	0.039195(1)
0.200	0.354(1)	0.1910(9)	0.0796(6)	0.0833(3)	0.074961(3)
0.250	0.420(2)	0.1802(9)	0.0990(9)	0.1411(9)	0.126308(8)
0.300	0.507(2)	0.1696(9)	0.118(1)	0.220(1)	0.196659(4)
0.350	0.623(3)	0.1588(9)	0.138(1)	0.326(2)	0.290175(6)
0.400	0.769(3)	0.1475(9)	0.157(2)	0.465(2)	0.41208(2)
0.450	0.958(4)	0.1367(7)	0.176(2)	0.646(3)	0.56872(1)
0.500	1.191(6)	0.1260(9)	0.192(2)	0.873(4)	0.76823(3)
0.550	1.488(7)	0.1152(6)	0.208(2)	1.165(6)	1.02060(5)
0.600	1.869(9)	0.1052(6)	0.224(2)	1.540(8)	1.33851(1)
0.650	2.35(1)	0.0949(6)	0.236(3)	2.02(1)	1.73807(3)
0.700	3.00(1)	0.0851(5)	0.243(3)	2.67(1)	2.24021(1)
0.750	3.86(2)	0.0763(4)	0.247(4)	3.54(2)	2.8712(2)
0.800	5.13(3)	0.0676(4)	0.244(4)	4.82(2)	3.6671(1)
0.850	7.17(4)	0.0595(3)	0.239(4)	6.87(4)	4.6717(1)
0.860	7.72(3)	0.0579(3)	0.234(3)	7.43(2)	4.9035(1)
0.870	8.37(4)	0.0562(3)	0.234(3)	8.08(4)	5.1461(1)
0.880	9.09(4)	0.0548(3)	0.229(5)	8.80(4)	5.4008(2)
0.890	9.97(4)	0.0535(2)	0.227(4)	9.69(4)	5.6677(1)
0.900	10.98(6)	0.0519(3)	0.223(5)	10.71(5)	5.9487(1)
0.910	12.15(6)	0.0506(3)	0.221(3)	11.88(6)	6.2434(1)
0.920	13.50(4)	0.0493(3)	0.216(4)	13.23(4)	6.5531(1)
0.930	15.19(7)	0.0480(4)	0.209(5)	14.93(7)	6.8796(3)
0.940	17.2(1)	0.0466(2)	0.208(6)	17.00(9)	7.2221(4)
0.950	19.6(1)	0.0456(3)	0.201(6)	19.34(9)	7.5841(4)
0.960	22.5(1)	0.0442(2)	0.196(4)	22.3(1)	7.9643(4)
0.970	26.0(1)	0.0431(3)	0.190(6)	25.8(1)	8.3659(1)
0.980	30.8(2)	0.0419(3)	0.186(5)	30.5(2)	8.790(1)
0.990	36.2(3)	0.0406(2)	0.181(7)	36.0(3)	9.239(1)
1.000	43.4(3)	0.0397(3)	0.179(6)	43.2(3)	9.714(1)
1.010	52.2(3)	0.0386(2)	0.170(9)	52.0(3)	10.215(1)
- solid below -					
1.000	4.0(2)	0.0485(3)	0.112(3)	3.8(2)	5.36960(7)
1.025	3.27(1)	0.0464(3)	0.136(2)	3.09(1)	5.81004(7)
1.050	3.31(2)	0.0441(2)	0.158(3)	3.11(1)	6.33799(1)
1.075	3.48(2)	0.0416(2)	0.179(2)	3.26(2)	6.96382(3)
1.100	3.71(2)	0.0392(2)	0.198(4)	3.48(2)	7.70516(1)
1.125	4.03(3)	0.0364(2)	0.217(3)	3.77(3)	8.58848(2)
1.150	4.42(1)	0.0338(2)	0.236(3)	4.15(1)	9.6515(1)
1.175	4.93(3)	0.0309(2)	0.251(2)	4.65(3)	10.9484(1)
1.200	5.56(3)	0.0280(1)	0.269(3)	5.26(3)	12.5601(1)
1.225	6.38(4)	0.0250(1)	0.286(3)	6.07(4)	14.6099(1)
1.250	7.44(4)	0.0219(1)	0.304(3)	7.11(4)	17.2968(2)
1.275	8.90(5)	0.0187(1)	0.320(4)	8.56(5)	20.9630(2)
1.300	10.99(5)	0.01550(8)	0.335(4)	10.64(5)	26.2509(1)
1.325	14.3(1)	0.01222(7)	0.354(4)	13.9(1)	34.5223(2)
1.350	20.2(1)	0.00886(5)	0.369(3)	19.8(1)	49.2618(5)
1.375	33.5(2)	0.00546(3)	0.385(3)	33.1(2)	82.8379(1)
1.400	93.8(3)	0.00200(1)	0.403(3)	93.4(3)	234.642(1)

TABLE V. Cross viscosity, η_{12}, and its components from the MD simulation as a function of density for the fluid and the solid phase (in units of $\sigma^{-2}(mk_BT)^{1/2}$)

ρ	η_{12}	η_{12}^{kk}	η_{12}^{kc}	η_{12}^{cc}	$\eta_{12}^{(I)}$
0.050	-0.1215(4)	-0.1125(3)	-0.0100(1)	0.0010(1)	0.001263(1)
0.100	-0.1219(5)	-0.1064(5)	-0.0199(1)	0.0044(1)	0.005410(1)
0.150	-0.1199(7)	-0.1009(5)	-0.0298(3)	0.0109(1)	0.013065(1)
0.200	-0.1139(7)	-0.0955(4)	-0.0398(3)	0.0213(3)	0.024986(1)
0.250	-0.103(1)	-0.0901(4)	-0.0495(4)	0.0370(7)	0.042104(1)
0.300	-0.086(1)	-0.0848(4)	-0.0589(5)	0.0580(9)	0.065556(1)
0.350	-0.061(2)	-0.0794(4)	-0.0689(6)	0.087(2)	0.096728(1)
0.400	-0.028(3)	-0.0737(5)	-0.0785(8)	0.124(2)	0.13735(1)
0.450	0.016(4)	-0.0683(3)	-0.0880(9)	0.173(3)	0.18957(1)
0.500	0.073(5)	-0.0629(5)	-0.096(1)	0.232(4)	0.25608(1)
0.550	0.144(5)	-0.0576(3)	-0.104(1)	0.305(5)	0.34022(1)
0.600	0.227(7)	-0.0526(3)	-0.112(1)	0.392(7)	0.44619(1)
0.650	0.33(1)	-0.0474(3)	-0.118(1)	0.49(1)	0.57936(2)
0.700	0.45(1)	-0.0426(3)	-0.122(1)	0.62(1)	0.74670(2)
0.750	0.61(2)	-0.0382(2)	-0.124(2)	0.78(2)	0.95706(9)
0.800	0.83(2)	-0.0338(2)	-0.122(2)	0.99(2)	1.22227(1)
0.850	1.20(3)	-0.0298(2)	-0.120(2)	1.35(3)	1.55705(6)
0.860	1.29(2)	-0.0290(2)	-0.117(1)	1.44(2)	1.63420(9)
0.870	1.44(3)	-0.0281(1)	-0.117(2)	1.58(3)	1.71494(5)
0.880	1.58(4)	-0.0274(2)	-0.114(2)	1.72(4)	1.79975(1)
0.890	1.80(3)	-0.0267(1)	-0.114(2)	1.94(3)	1.88848(2)
0.900	2.04(5)	-0.0260(2)	-0.112(3)	2.18(5)	1.98208(4)
0.910	2.36(5)	-0.0253(2)	-0.110(2)	2.50(5)	2.08002(1)
0.920	2.73(5)	-0.0247(1)	-0.108(2)	2.87(5)	2.18318(2)
0.930	3.24(6)	-0.0240(2)	-0.104(3)	3.37(6)	2.29170(7)
0.940	3.89(8)	-0.0233(1)	-0.104(3)	4.02(8)	2.4061(2)
0.950	4.70(8)	-0.0228(2)	-0.101(3)	4.83(8)	2.5267(1)
0.960	5.68(7)	-0.0221(1)	-0.098(2)	5.80(7)	2.6540(1)
0.970	7.0(1)	-0.0215(1)	-0.095(3)	7.1(1)	2.7881(1)
0.980	8.8(2)	-0.0209(1)	-0.093(3)	8.9(2)	2.9300(1)
0.990	10.9(2)	-0.0203(1)	-0.091(3)	11.0(2)	3.0800(5)
1.000	14.0(2)	-0.0198(1)	-0.089(3)	14.1(2)	3.2378(1)
1.010	18.0(2)	-0.0193(1)	-0.087(5)	18.1(2)	3.4050(5)
			- solid below -		
1.000	-0.1(2)	-0.0242(1)	-0.056(1)	-0.1(2)	2.53350(2)
1.025	-1.040(9)	-0.0232(1)	-0.068(1)	-0.949(8)	2.77338(3)
1.050	-1.283(8)	-0.0220(1)	-0.079(2)	-1.182(7)	3.05281(1)
1.075	-1.486(9)	-0.0208(1)	-0.089(1)	-1.376(9)	3.37861(1)
1.100	-1.67(1)	-0.0196(1)	-0.099(2)	-1.56(1)	3.76047(1)
1.125	-1.88(2)	-0.0182(1)	-0.108(2)	-1.75(2)	4.21214(2)
1.150	-2.11(1)	-0.0169(1)	-0.118(1)	-1.97(1)	4.75279(6)
1.175	-2.38(2)	-0.0155(1)	-0.125(1)	-2.24(1)	5.40974(3)
1.200	-2.72(1)	-0.01401(6)	-0.135(2)	-2.57(1)	6.22354(1)
1.225	-3.14(2)	-0.01249(7)	-0.143(2)	-2.99(2)	7.25596(5)
1.250	-3.68(2)	-0.01096(6)	-0.152(2)	-3.52(2)	8.60658(7)
1.275	-4.42(3)	-0.00937(5)	-0.160(2)	-4.25(2)	10.44660(8)
1.300	-5.47(3)	-0.00775(4)	-0.168(2)	-5.30(3)	13.09722(1)
1.325	-7.13(5)	-0.00611(4)	-0.177(2)	-6.95(5)	17.2394(1)
1.350	-10.06(5)	-0.00443(2)	-0.185(2)	-9.87(5)	24.6154(2)
1.375	-16.75(8)	-0.00273(1)	-0.192(1)	-16.55(8)	41.4096(1)
1.400	-46.9(1)	-0.000997(4)	-0.202(2)	-46.7(1)	117.3176(7)

TABLE VI. Shear viscosity, η_{44}, and its components obtained by MD as a function of density for the fluid and the solid phase (in units of $\sigma^{-2}(mk_BT)^{1/2}$)

| ρ	η_{44}	η_{44}^{kk}	η_{44}^{kc}	η_{44}^{cc}	$\eta_{44}^{(I)}$
0.050	0.1854(3)	0.1688(3)	0.0150(1)	0.00159(1)	0.001263(1)
0.100	0.1965(5)	0.1598(5)	0.0299(1)	0.00676(2)	0.005410(1)
0.150	0.2121(6)	0.1511(5)	0.0447(3)	0.01624(5)	0.013065(1)
0.200	0.234(1)	0.1430(6)	0.0596(5)	0.0310(1)	0.024986(1)
0.250	0.261(1)	0.1352(6)	0.0741(4)	0.0521(2)	0.042104(1)
0.300	0.297(1)	0.1271(5)	0.0889(7)	0.0811(4)	0.065556(1)
0.350	0.341(2)	0.1189(6)	0.1030(9)	0.1194(5)	0.096728(1)
0.400	0.398(2)	0.1106(4)	0.1170(9)	0.1701(9)	0.13735(1)
0.450	0.469(3)	0.1027(5)	0.131(1)	0.235(1)	0.18957(1)
0.500	0.559(3)	0.0941(4)	0.144(1)	0.321(2)	0.25608(1)
0.550	0.673(3)	0.0864(4)	0.157(1)	0.430(2)	0.34022(1)
0.600	0.818(4)	0.0785(4)	0.167(2)	0.572(3)	0.44619(1)
0.650	1.011(5)	0.0711(4)	0.176(2)	0.764(4)	0.57936(2)
0.700	1.274(7)	0.0640(3)	0.184(2)	1.026(5)	0.74670(2)
0.750	1.628(6)	0.0571(2)	0.186(2)	1.386(6)	0.95706(9)
0.800	2.15(1)	0.0508(3)	0.185(2)	1.92(1)	1.22227(1)
0.850	2.99(2)	0.0448(2)	0.178(2)	2.77(1)	1.55705(6)
0.860	3.23(1)	0.0431(2)	0.177(2)	3.00(1)	1.63420(9)
0.870	3.47(2)	0.0420(2)	0.174(2)	3.26(1)	1.71494(5)
0.880	3.76(2)	0.0410(2)	0.173(3)	3.55(2)	1.79975(1)
0.890	4.10(2)	0.0399(2)	0.171(2)	3.89(2)	1.88848(2)
0.900	4.44(2)	0.0389(2)	0.166(3)	4.24(2)	1.98208(4)
0.910	4.89(2)	0.0379(2)	0.164(2)	4.69(2)	2.08002(1)
0.920	5.37(3)	0.0369(2)	0.160(4)	5.18(3)	2.18318(2)
0.930	5.96(2)	0.0359(2)	0.159(3)	5.77(2)	2.29170(7)
0.940	6.64(4)	0.0350(2)	0.153(4)	6.45(4)	2.4061(2)
0.950	7.44(3)	0.0340(2)	0.151(4)	7.26(3)	2.5267(1)
0.960	8.42(4)	0.0331(2)	0.147(4)	8.24(4)	2.6540(1)
0.970	9.54(5)	0.0321(2)	0.144(3)	9.36(4)	2.7881(1)
0.980	10.91(5)	0.0313(1)	0.141(5)	10.74(5)	2.9300(1)
0.990	12.60(7)	0.0304(1)	0.136(5)	12.44(7)	3.0800(5)
1.000	14.62(8)	0.0297(2)	0.135(5)	14.45(8)	3.2378(5)
1.010	17.08(9)	0.0288(2)	0.133(6)	16.91(9)	3.4050(5)
			- solid below -		
1.000	3.83(2)	0.0501(2)	0.555(3)	3.23(1)	2.53350(2)
1.025	4.16(2)	0.0485(2)	0.583(2)	3.53(1)	2.77338(3)
1.050	4.55(2)	0.0465(2)	0.609(3)	3.89(2)	3.05281(1)
1.075	5.00(2)	0.0442(2)	0.631(3)	4.32(2)	3.37861(1)
1.100	5.54(2)	0.0418(2)	0.658(4)	4.84(2)	3.76047(1)
1.125	6.15(4)	0.0391(2)	0.679(4)	5.44(4)	4.21214(2)
1.150	6.90(4)	0.0363(1)	0.703(3)	6.16(4)	4.75279(6)
1.175	7.82(6)	0.0333(2)	0.726(6)	7.06(6)	5.40974(3)
1.200	8.93(4)	0.0303(2)	0.747(4)	8.15(3)	6.22354(1)
1.225	10.37(3)	0.0271(1)	0.772(3)	9.57(3)	7.25596(5)
1.250	12.20(5)	0.0238(1)	0.793(4)	11.39(5)	8.60658(7)
1.275	14.71(6)	0.0204(1)	0.814(5)	13.87(6)	10.44660(8)
1.300	18.31(7)	0.01697(7)	0.837(3)	17.46(7)	13.09722(1)
1.325	24.0(1)	0.01341(6)	0.859(6)	23.1(1)	17.2394(1)
1.350	34.0(1)	0.00973(3)	0.880(3)	33.1(1)	24.6154(2)
1.375	56.8(2)	0.00601(2)	0.902(3)	55.9(2)	41.4096(1)
1.400	160.2(7)	0.00220(1)	0.926(4)	159.2(7)	117.3176(7)
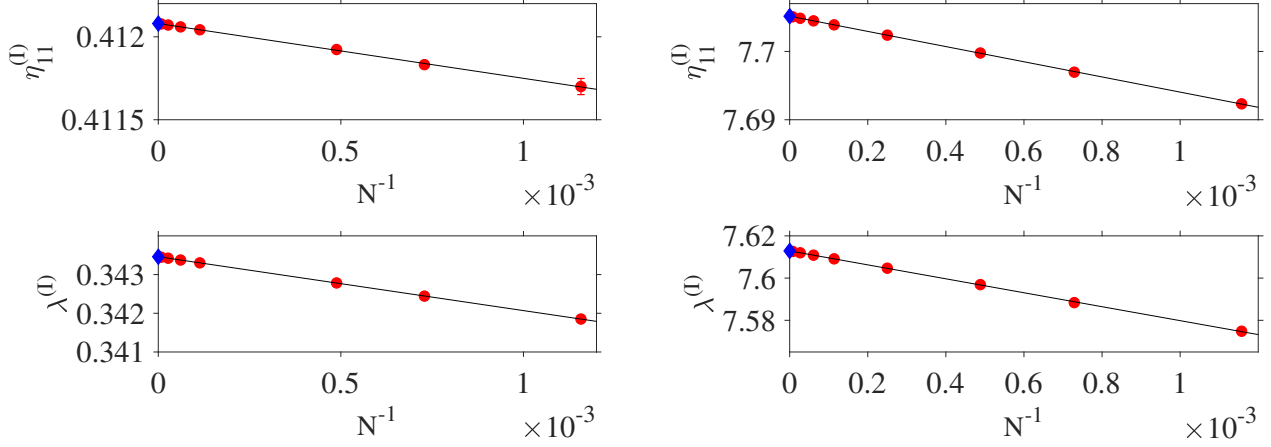
FIG. 12. The N-dependence of the instantaneous (I) part of η_{11} and λ for fluid $\rho = 0.4$ (left figures) and solid $\rho = 1.1$ (right figures) densities. The solid red points are the MD values for $N = 864, 1372, 2048, 4000, 8788, 16384, 37044$ and 131072. The solid black lines are the linear fits to the data. The solid blue diamond represents the value of each transport coefficient in the thermodynamic limit.
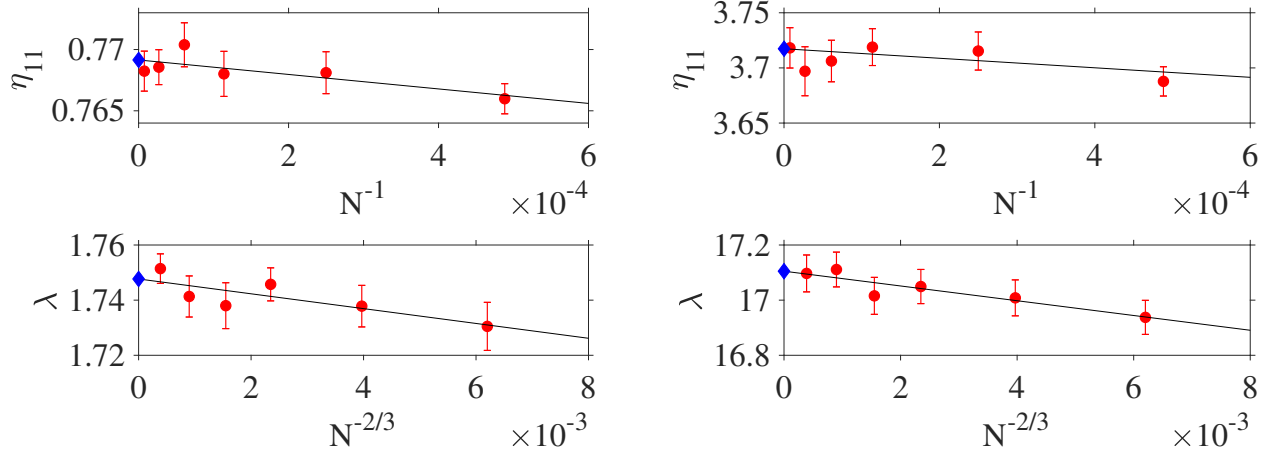

FIG. 13. Same as in Fig. 12, except that in this instance the total value of transport coefficients are presented.

vectors $\mathbf{G}$ in the summations and the three-body direct correlation function.

The resultant elastic terms, $\mathcal{E}_p$,

$$\mathcal{E}_1 = \frac{C_{44}^{u\alpha}}{C_{44}^{\alpha\alpha}}, \tag{C3a}$$

$$\mathcal{E}_2 = \frac{C_{11}^{u\alpha} + 2C_{12}^{u\alpha}}{C_{11}^{\alpha\alpha} + 2C_{12}^{\alpha\alpha}}, \tag{C3b}$$

$$\mathcal{E}_3 = \frac{C_{11}^{u\alpha} - C_{12}^{u\alpha}}{C_{11}^{\alpha\alpha} - C_{12}^{\alpha\alpha}}, \tag{C3c}$$

are presented in Figure 14.

Appendix D: Estimation of the elastic terms at high densities from the H integrals

The DFT elastic coefficients necessary to determine the $\mathcal{E}_p$ are as follows in terms of the H-functions (for more details see Appendix B in Ref. 8),

$$C_{ijkl}^{u\alpha} = \frac{\rho a^2}{4k_BT}\left[\delta_{ij}H_{kl}^{(2)} + H_{ijkl}^{(3)}\right], \tag{D1}$$

$$C_{ijkl}^{\alpha\alpha} = \frac{\rho a^4}{16k_BT}\left[H_{ijkl}^{(5)} - H_{ijkl}^{(6)}\right], \tag{D2}$$

where,

$$H_{ij}^{(2)} = \frac{1}{\rho V}\int d\mathbf{r}_1 d\mathbf{r}_2 c(\mathbf{r}_1,\mathbf{r}_2)\varrho(\mathbf{r}_1)\frac{\partial^2\varrho(\mathbf{r}_2)}{\partial r_{2i}\partial r_{2j}}, \tag{D3}$$

TABLE VII. Bulk viscosity, η_B, and its I part obtained by MD as a function of density for the fluid and the solid phase (in units of $\sigma^{-2}(mk_BT)^{1/2}$)

| ρ	η_B	$\eta_B^{(I)}$
0.050	0.00208(1)	0.002105(1)
0.100	0.00890(4)	0.009017(1)
0.150	0.0217(1)	0.021775(1)
0.200	0.0420(2)	0.041645(2)
0.250	0.0717(7)	0.070172(2)
0.300	0.1119(9)	0.109257(1)
0.350	0.167(2)	0.161210(3)
0.400	0.238(2)	0.22893(1)
0.450	0.330(3)	0.31596(1)
0.500	0.446(4)	0.42680(1)
0.550	0.592(5)	0.56701(2)
0.600	0.774(7)	0.74363(1)
0.650	1.00(1)	0.96559(2)
0.700	1.30(1)	1.24453(1)
0.750	1.70(2)	1.59510(9)
0.800	2.26(2)	2.03722(1)
0.850	3.19(3)	2.59528(1)
0.860	3.43(2)	2.72395(9)
0.870	3.75(3)	2.85867(7)
0.880	4.08(3)	3.00008(5)
0.890	4.52(3)	3.14822(2)
0.900	5.02(5)	3.30430(9)
0.910	5.62(5)	3.46782(5)
0.920	6.32(4)	3.63982(4)
0.930	7.22(5)	3.8210(1)
0.940	8.34(8)	4.0114(2)
0.950	9.66(8)	4.2123(1)
0.960	11.29(7)	4.4240(1)
0.970	13.3(1)	4.6475(1)
0.980	16.1(2)	4.8836(5)
0.990	19.3(2)	5.1333(6)
1.000	23.8(2)	5.3964(5)
1.010	29.4(2)	5.6751(6)
- solid below -		
1.000	1.2(2)	3.47887(4)
1.025	0.397(3)	3.78560(5)
1.050	0.249(2)	4.14787(2)
1.075	0.170(2)	4.57367(2)
1.100	0.121(1)	5.07536(1)
1.125	0.090(1)	5.67092(2)
1.150	0.0689(7)	6.38569(8)
1.175	0.0535(8)	7.25597(4)
1.200	0.0417(7)	8.33573(3)
1.225	0.0327(3)	9.70727(7)
1.250	0.0250(4)	11.50333(7)
1.275	0.0194(4)	13.95210(9)
1.300	0.0150(6)	17.48176(4)
1.325	0.0105(5)	23.0004(1)
1.350	0.0082(8)	32.8309(3)
1.375	0.0036(9)	55.2190(1)
1.400	0.005(3)	156.4257(9)
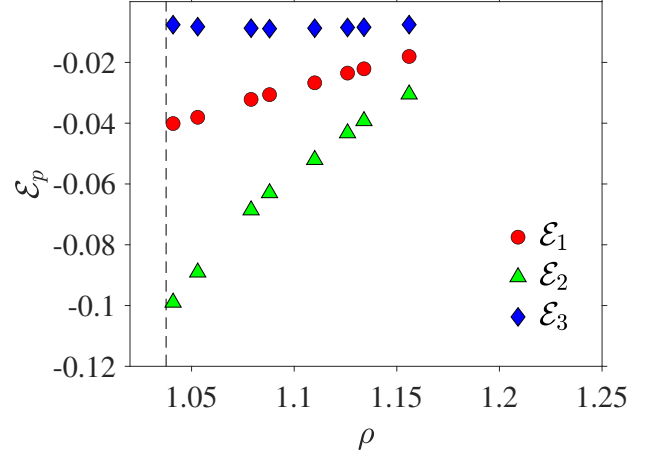
FIG. 14. The density dependence of the elastic terms $\mathcal{E}_i$ calculated from the DFT approach using Eq. (C3) are presented for densities up to $\rho \sim 1.15$. The vertical thin dashed line indicates the melting ($\rho_m = 1.0376$) density.

$$H_{ijkl}^{(3)} = \frac{1}{2\rho V} \int d\mathbf{r}_1 d\mathbf{r}_2 c(\mathbf{r}_1, \mathbf{r}_2) \left(r_{12j} \right.$$
$$\left. \times \frac{\partial \varrho(\mathbf{r}_1)}{\partial r_{1i}} + r_{12i} \frac{\partial \varrho(\mathbf{r}_1)}{\partial r_{1j}} \right) \frac{\partial^2 \varrho(\mathbf{r}_2)}{\partial r_{2k} \partial r_{2l}}, \quad \text{(D4)}$$

$$H_{ijkl}^{(5)} = \frac{1}{\rho V} \int d\mathbf{r}_1 \frac{\partial^2 \varrho(\mathbf{r}_1)}{\partial r_{1i} \partial r_{1j}} \left[\varrho(\mathbf{r}_1) \right]^{-1} \frac{\partial^2 \varrho(\mathbf{r}_1)}{\partial r_{1k} \partial r_{1l}}, \text{(D5)}$$

$$H_{ijkl}^{(6)} = \frac{1}{\rho V} \int d\mathbf{r}_1 d\mathbf{r}_2 c(\mathbf{r}_1, \mathbf{r}_2)$$
$$\times \frac{\partial^2 \varrho(\mathbf{r}_1)}{\partial r_{1i} \partial r_{1j}} \frac{\partial^2 \varrho(\mathbf{r}_2)}{\partial r_{2k} \partial r_{2l}}. \quad \text{(D6)}$$

With the Gaussian approximation for the one-particle density distribution $\varrho(\mathbf{r}) = \pi^{-3/2} \alpha^{-3/2} a^{-3} \exp(-(\mathbf{R} - \mathbf{r})^2/a^2\alpha)$ the functions $H_{ijkl}^{(5)}$ can be calculated exactly but other H-functions require the DCF of a hard sphere crystal.

At high densities each particle is strongly localized near its average lattice site position, $\mathbf{R}$, which means, taking into account the short-ranged nature of the DCF, that the product $\varrho(\mathbf{r}_1)\varrho(\mathbf{r}_2)c(\mathbf{r}_1, \mathbf{r}_2)$ is practically nonzero only for small deviations from one site ($\delta\mathbf{r}_1, \delta\mathbf{r}_2$) and for small distances from near-neighbor two-sites ($\delta\mathbf{r}_1, \mathbf{R}_{12} + \delta\mathbf{r}_2$). These two situations represent, to a large extent, the main contributions to each H-function at high densities and thus can be formulated by the following approximation,

$$c(\mathbf{r}_1, \mathbf{r}_2) = C_1(\delta\mathbf{r}_1, \delta\mathbf{r}_2)N + C_2(\delta\mathbf{r}_1, \mathbf{R}_{12} + \delta\mathbf{r}_2)NN_s, \quad \text{(D7)}$$

where N, N_s are the number of particles and number of nearest neighbors (12 in an fcc crystal).

TABLE VIII. The thermal conductivity, λ, and its components (in units of $k_B \sigma^{-2}(k_B T/m)^{1/2}$) of the HS fluid and solid obtained by extrapolating the MD data to the thermodynamic limit. The three points at very low density for the cc part of the thermal conductivity have been corrected compared to the same values in Table 1 in Ref. 27.

ρ	λ	λ^{kk}	λ^{kc}	λ^{cc}	λ^{I}
0.050	0.730(1)	0.639(1)	0.0849(2)	0.00602(1)	0.003157(1)
0.100	0.798(2)	0.602(2)	0.1694(6)	0.02582(8)	0.013526(1)
0.150	0.882(2)	0.567(2)	0.2531(8)	0.0623(2)	0.032665(2)
0.200	0.994(5)	0.535(2)	0.339(2)	0.1197(6)	0.062463(7)
0.250	1.128(4)	0.502(2)	0.424(2)	0.2020(8)	0.105261(8)
0.300	1.298(5)	0.470(2)	0.512(2)	0.316(1)	0.163886(5)
0.350	1.493(5)	0.434(1)	0.594(2)	0.466(2)	0.241815(8)
0.400	1.748(7)	0.402(2)	0.682(3)	0.664(3)	0.34346(3)
0.450	2.061(9)	0.371(2)	0.770(5)	0.920(4)	0.47403(1)
0.500	2.44(1)	0.340(2)	0.858(6)	1.246(7)	0.64015(3)
0.550	2.91(1)	0.308(2)	0.942(6)	1.660(8)	0.8506(1)
0.600	3.50(2)	0.280(1)	1.032(6)	2.19(1)	1.1154(1)
0.650	4.23(3)	0.253(2)	1.122(8)	2.85(2)	1.4483(2)
0.700	5.12(2)	0.226(1)	1.206(7)	3.69(2)	1.8667(2)
0.750	6.23(3)	0.200(1)	1.290(9)	4.74(2)	2.3928(1)
0.800	7.64(4)	0.1776(9)	1.380(9)	6.08(3)	3.0557(2)
0.850	9.39(4)	0.1551(7)	1.472(8)	7.77(4)	3.8925(1)
0.860	9.79(5)	0.1505(6)	1.490(8)	8.15(4)	4.0857(1)
0.870	10.22(4)	0.1466(7)	1.509(6)	8.56(4)	4.2879(1)
0.880	10.64(5)	0.1426(7)	1.526(9)	8.97(4)	4.5000(1)
0.890	11.14(6)	0.1390(7)	1.548(9)	9.45(5)	4.7220(1)
0.900	11.58(5)	0.1349(6)	1.562(9)	9.89(4)	4.9563(1)
0.910	12.08(6)	0.1318(6)	1.58(1)	10.36(5)	5.2012(5)
0.920	12.59(7)	0.1274(8)	1.60(1)	10.87(6)	5.4598(2)
0.930	13.19(6)	0.1240(7)	1.62(1)	11.44(5)	5.7313(1)
0.940	13.78(8)	0.1205(7)	1.64(1)	12.02(7)	6.0174(6)
0.950	14.29(7)	0.1167(7)	1.65(1)	12.52(6)	6.3184(2)
0.960	14.96(7)	0.1133(5)	1.67(1)	13.17(6)	6.6370(9)
0.970	15.6(1)	0.1094(7)	1.69(1)	13.84(9)	6.9733(1)
0.980	16.3(1)	0.1068(7)	1.72(2)	14.5(1)	7.3248(9)
0.990	17.0(1)	0.1030(9)	1.72(1)	15.1(1)	7.6980(8)
1.000	17.7(1)	0.0992(8)	1.73(2)	15.8(1)	8.0946(9)
1.010	18.6(1)	0.0962(5)	1.76(1)	16.7(1)	8.5126(8)
			- solid below -		
1.000	12.23(4)	0.1412(6)	1.931(7)	10.16(3)	5.2182(1)
1.025	13.14(5)	0.1349(6)	1.983(9)	11.03(4)	5.6787(1)
1.050	14.28(8)	0.1291(6)	2.05(1)	12.10(7)	6.2216(1)
1.075	15.55(5)	0.1218(4)	2.10(1)	13.33(5)	6.8607(1)
1.100	17.11(8)	0.1148(5)	2.16(1)	14.83(7)	7.6129(2)
1.125	19.0(1)	0.1071(7)	2.22(2)	16.7(1)	8.5064(5)
1.150	21.1(1)	0.0987(3)	2.27(1)	18.7(1)	9.5784(2)
1.175	23.7(2)	0.0908(5)	2.33(2)	21.3(1)	10.8841(6)
1.200	27.0(2)	0.0823(4)	2.38(1)	24.5(1)	12.5040(3)
1.225	31.1(1)	0.0735(2)	2.44(1)	28.6(1)	14.5615(2)
1.250	36.3(2)	0.0643(4)	2.49(1)	33.8(2)	17.2541(2)
1.275	43.8(2)	0.0551(3)	2.55(1)	41.2(1)	20.9280(5)
1.300	54.2(3)	0.0456(2)	2.61(1)	51.6(3)	26.2205(7)
1.325	70.5(4)	0.0359(2)	2.66(1)	67.8(4)	34.5016(1)
1.350	99.8(5)	0.0262(1)	2.72(1)	97.0(5)	49.246(2)
1.375	166.1(7)	0.01606(9)	2.77(1)	163.3(7)	82.833(4)
1.400	466(2)	0.00589(2)	2.83(1)	464(2)	234.64(2)

From the work in Ref. 31 it follows that for small deviations from any site the DCF is almost constant and to a good approximation, isotropic. This observation may be cast into an approximation formula for the one-site contribution,

$$C_1(\delta\mathbf{r}_1, \delta\mathbf{r}_2) = C_1(0,0) + w_1|\delta\mathbf{r}_1| + w_2|\delta\mathbf{r}_1||\delta\mathbf{r}_2|, \quad \text{(D8)}$$

where w_1, w_2 represents the first and second derivatives of the DCF at the site position. For high densities the departures from the site position are very small and for small departures or distances the DCF is almost constant. The DCF is a function which hardly changes with distance [31], which means that the slopes w_1 and w_2 can be expected to be small or moderate numbers which we assume are (considerably) less than $1/\alpha$.

For the two-site contribution a second order Taylor expansion is used,

$$C_2(\delta\mathbf{r}_1, \mathbf{R}_{12} + \delta\mathbf{r}_2) = C_2(0, \mathbf{R}_{12}) + \sum_{i=1}^{6} K_i^{(1)}\delta X_i$$
$$+ \sum_{i=1}^{6}\sum_{j=1}^{6} K_{ij}^{(2)}\delta X_i \delta X_j, \quad \text{(D9)}$$

where δX_1, δX_2, ... δX_6 stands here for the Cartesian increment δx_1, δy_1, δz_1, δx_2, δy_2, δz_2. $K^{(1)}$, $K^{(2)}$ denote the corresponding first and second order derivatives and are considered here to be unknown constants of magnitude less than $1/\alpha$ (like w_1, w_2). For example, the K-derivatives are $K_1^{(1)} = \partial c(\mathbf{r}_1, \mathbf{r}_2)/\partial\delta x_1$ and $K_{11}^{(2)} = \partial c(\mathbf{r}_1, \mathbf{r}_2)/\partial\delta x_1\partial\delta x_1$.

For the model in Eqs. (D7) - (D9) and the Gaussian approximation for the one-particle distribution, $\varrho(\mathbf{r}_1)$, the H-functions can be calculated, and the results for the required function are as follows,

$$H_{11}^{(2)} = \frac{8w_2}{3\pi} + 16K_{44}^{(2)}, \quad \text{(D10)}$$

$$H_{11}^{(2)} = \frac{8w_2}{3\pi} + 16K_{55}^{(2)}, \quad \text{(D11)}$$

$$H_{1111}^{(3)} = -\frac{32w_2}{9\pi} + 16\left(K_{14}^{(2)} + K_{41}^{(2)} - K_{44}^{(2)}\right) \text{(D12)}$$

$$H_{1122}^{(3)} = -\frac{32w_2}{9\pi} - 16K_{55}^{(2)}, \quad \text{(D13)}$$

$$H_{1212}^{(3)} = 4\left(K_{14}^{(2)} + K_{41}^{(2)} + K_{25}^{(2)} + K_{52}^{(2)}\right), \quad \text{(D14)}$$

$$H_{1111}^{(5)} = \frac{8}{a^4\alpha^2}, \quad H_{1122}^{(5)} = 0, \quad H_{1212}^{(5)} = \frac{4}{a^4\alpha^2}, \text{(D15)}$$

$$H_{1111}^{(6)} = \frac{16w_2}{9\pi a^2\alpha}, \quad H_{1122}^{(6)} = \frac{16w_2}{9\pi a^2\alpha}, \quad H_{1212}^{(6)} = 0 \text{(D16)}$$

From the above H-functions the elastic components in Eqs. (D1) and (D2) are calculated and the $\mathcal{E}_p$ functions from the expressions in Eqs. (C3) are obtained,

$$\mathcal{E}_1 = 4a^2\alpha^2\left(K_{14}^{(2)} + K_{41}^{(2)} + K_{25}^{(2)} + K_{52}^{(2)}\right) \text{(D17a)}$$

$$\mathcal{E}_2 = 4a^2\alpha^2\frac{w_2 - 6\pi(K_{14}^{(2)} + K_{41}^{(2)})}{2a^2\alpha w_2 - 3\pi}$$
$$= \frac{4a^2\alpha^2}{3\pi}\left(6\pi(K_{14}^{(2)} + K_{41}^{(2)}) - w_2\right), \quad \text{(D17b)}$$

$$\mathcal{E}_3 = 8a^2\alpha^2\left(K_{14}^{(2)} + K_{41}^{(2)}\right), \quad \text{(D17c)}$$

where the second equality in Eq. (D17b) is from the assumed relation $w_2 \ll 1/\alpha$. Thus, in the dense HS solid the elastic components $\mathcal{E}_p/\alpha$ are estimated to be $\sim \alpha$ or at least a bounded quantity.

[1] J. R. Dorfman, H. van Beijeren, and T. R. Kirkpatrick, *Contemporary Kinetic Theory of Matter* (Cambridge University Press, 2021).

[2] S. Chapman and T. G. Cowling, *The Mathematical Theory of Non-Uniform Gases* (Cambridge University Press, 1991).

[3] S. Loyalka, E. Tipton, and R. Tompson, Physica A **379**, 417 (2007).

[4] P. Résibois and M. Leener, *Classical kinetic theory of fluids* (Wiley, New York, 1977).

[5] H. van Beijeren and M. H. Ernst, Physica **68**, 437 (1973).

[6] M. L. de Haro and E. G. D. Cohen, The Journal of Chemical Physics **80**, 408 (1984).

[7] J. M. Kincaid, E. G. D. Cohen, and M. L. de Haro, The Journal of Chemical Physics **86**, 963 (1987).

[8] T. R. Kirkpatrick, S. P. Das, M. H. Ernst, and J. Piasecki, The Journal of Chemical Physics **92**, 3768 (1990).

[9] S. Viscardy and P. Gaspard, Physical Review E **68**, 041204 (2003).

[10] D. C. Wallace, *Thermodynamics of crystals* (Dover Publications, 1998).

[11] M. H. Ernst and R. Brito, Physical Review E **72**, 061102 (2005).

[12] M. P. Allen and D. J. Tildesley, *Computer Simulation of Liquids* (Oxford University Press, 2017).

[13] J. M. Haile, *Molecular dynamics simulation* (Wiley, New

York, 1997).

[14] J. J. Erpenbeck, Physical Review E **51**, 4296 (1995).

[15] E. Helfand, Physical Review **119**, 1 (1960).

[16] D. M. Heyes, S. Pieprzyk, and A. C. Brańka, The Journal of Chemical Physics **157**, 10.1063/5.0101728 (2022).

[17] J. W. Dufty, Molecular Physics **100**, 2331 (2002).

[18] J. W. Dufty, Granular Matter **14**, 271 (2011).

[19] A. C. Brańka and D. M. Heyes, Physical Review E **69**, 021202 (2004).

[20] There is a typographical error in eqs. (7) and (14) of ref. [16]; the denominators should be r and not r^2.

[21] M. N. Bannerman, R. Sargant, and L. Lue, J. Comput. Chem. **32**, 3329 (2011).

[22] S. Pieprzyk, M. N. Bannerman, A. C. Brańka, M. Chudak, and D. M. Heyes, Physical Chemistry Chemical Physics **21**, 6886 (2019).

[23] M. Fushiki, Physical Review E **68**, 021203 (2003).

[24] I.-C. Yeh and G. Hummer, The Journal of Physical Chemistry B **108**, 15873 (2004).

[25] D. M. Heyes, M. J. Cass, J. G. Powles, and W. A. B. Evans, The Journal of Physical Chemistry B **111**, 1455 (2007).

[26] K.-S. Kim, M. H. Han, C. Kim, Z. Li, G. E. Karniadakis, and E. K. Lee, The Journal of Chemical Physics **149**, 10.1063/1.5035119 (2018).

[27] S. Pieprzyk, A. Brańka, D. Heyes, and M. Bannerman, Phys. Chem. Chem. Phys. **22**, 8834 (2020).

[28] S. K. Loyalka, E. L. Tipton, and R. V. Tompson, Physica A: Statistical Mechanics and its Applications **379**, 417 (2007).

[29] H. Sigurgeirsson and D. M. Heyes, Molecular Physics **101**, 469 (2003).

[30] M. V. Jaric and U. Mohanty, Phys. Rev. B **37**, 4441 (1988).

[31] S. C. Lin, M. Oettel, J. M. Häring, R. Haussmann, M. Fuchs, and G. Kahl, Phys. Rev. Lett. **127**, 085501 (2021).

[32] S. W. Smith, C. K. Hall, and B. D. Freeman, The Journal of Chemical Physics **102**, 1057 (1995).

[33] B. J. Alder, D. M. Gass, and T. E. Wainwright, The Journal of Chemical Physics **53**, 3813 (1970).

[34] J.-M. Bomont and J.-L. Bretonnet, Chemical Physics **439**, 85 (2014).

[35] R. Srivastava, D. Dwivedee, and K. Khanna, Journal of Molecular Liquids **139**, 29 (2008).

[36] J. J. Erpenbeck and W. W. Wood, Physical Review A **43**, 4254 (1991).

[37] J. J. Erpenbeck and W. W. Wood, Journal of Statistical Physics **24**, 455 (1981).

[38] E. J. Le Fevre, Nature Physical Science **235**, 20 (1972).

[39] G. Szamel and M. H. Ernst, Physical Review B **48**, 112 (1993).

[40] N. Sushko, P. van der Schoot, and M. A. J. Michels, The Journal of Chemical Physics **118**, 6594 (2003).

[41] S. L. Singh, A. S. Bharadwaj, and Y. Singh, Physical Review E **83**, 051506 (2011).

[42] A. Manacorda, G. Schehr, and F. Zamponi, The Journal of Chemical Physics **152**, 10.1063/5.0007036 (2020).

[43] See supplemental material at [url will be inserted by publisher] where the molecular dynamic data is provided as text files.

[44] N. Sushko, P. van der Schoot, and M. A. J. Michels, The Journal of Chemical Physics **115**, 7744 (2001).